SIEMENS

Imaging Life

The Magazine for Molecular Imaging Innovation

June 2014 | Clinical Case Supplement

Biograph mCT Flow:

Detection of Brain Metastases using Hi-Rez Reconstruction and FlowMotion Technology

Page 4

Biograph mCT 64

^{82}Rb PET•CT Myocardial Perfusion and Blood Flow Evaluation

Page 16

Symbia Intevo

Delineation of Femoral Marrow Infiltration using xSPECT Bone and CT

Page 32

Mario Zeiss
Vice President
Global Marketing and Sales
Molecular Imaging, Siemens Healthcare

Dear Reader,

This *Imaging Life Clinical Case Supplement* from Siemens Molecular Imaging reflects the desire and initiative of our organization to highlight the innovative clinical work our global customers are performing with their Siemens Biograph™ and Symbia™ systems in the expanding field of molecular imaging.

In support of the growth of our industry, Siemens Molecular Imaging would like to share the best practices of our users and help stimulate new ideas with a broader clinical audience. We strive to provide a forum for our users from which they can transfer clinical knowledge and insights as a way to promote molecular imaging techniques and stimulate the interest of referring physicians and new adopters.

As part of our ongoing commitment to innovation leadership, Siemens Molecular Imaging recently introduced the concept of FlowMotion™—PET acquisition with continuous bed motion, which is available on the Biograph mCT Flow™* PET•CT system. Likewise, we helped revolutionize SPECT/CT, with the introduction of the xSPECT**, a new modality that completely integrates SPECT and CT data during reconstruction. Presented in several case studies, this publication highlights the clinical impact and value of these new technological innovations.

We hope you enjoy reading this collection of case studies. As always, we would appreciate your feedback and look forward to continue working with you to help bring the benefits of molecular imaging to even more patients around the world.

Best regards,

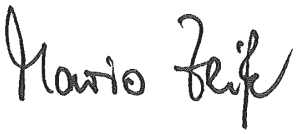

Mario Zeiss
Vice President, Global Marketing and Sales
Molecular Imaging, Siemens Healthcare

* Biograph mCT Flow is not commercially available in all countries. Due to regulatory reasons, its future availability cannot be guaranteed. Please contact your local Siemens organization for further details.

** Symbia Intevo and xSPECT are not commercially available in all countries. Due to regulatory reasons, their future availability cannot be guaranteed. Please contact your local Siemens organization for further details.

Table of Contents

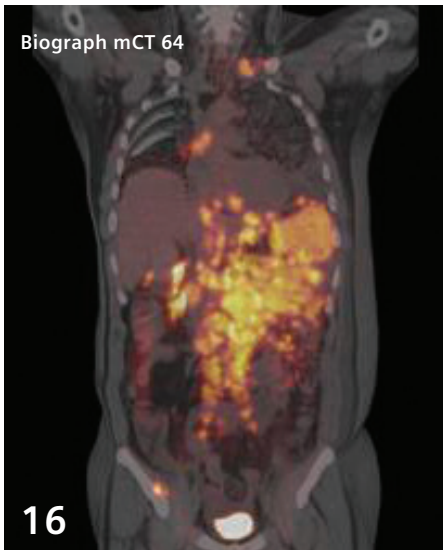

^{82}Rb PET•CT Myocardial Perfusion and Blood Flow Evaluation

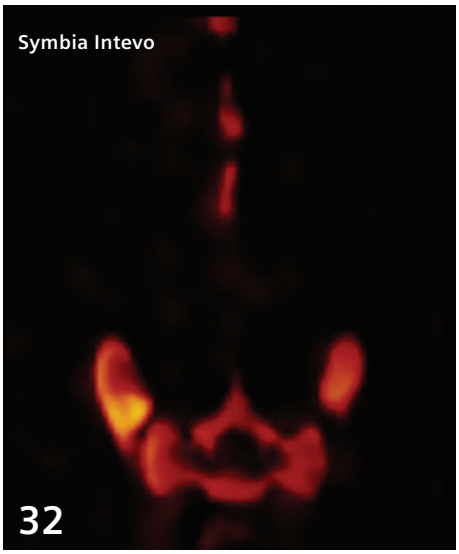

Delineation of Femoral Marrow Infiltration using xSPECT Bone and CT

Imaging Life

Everything from the world of molecular imaging innovations. As a supplement to *Imaging Life*, this publication presents clinical case studies from Siemens Molecular Imaging's customers as a way to share clinical insights with the global molecular imaging community.

Clinical Case Studies

Detection of Brain Metastases in a Patient with Breast Carcinoma with ^{18}F FDG* PET•CT using Hi-Rez Reconstruction and FlowMotion Technology

By: **Partha Ghosh, MD, Molecular Imaging Business Unit, Siemens Healthcare**

Data courtesy of University of Michigan, Ann Arbor, MI, USA

History

A 54-year-old female patient with history of adenocarcinoma of the left breast, treated with mastectomy with axillary clearance, underwent Fludeoxyglucose F 18 (^{18}F FDG) PET•CT for follow up. The patient complained of right-side weakness for which she underwent a CT scan of the brain that showed a suspicious space-occupying lesion in the left basal ganglial region. PET•CT was recommended to evaluate for metastases.

A PET•CT study was performed 1 hour following IV administration of 8 mCi of ^{18}F FDG. FlowMotion™ acquisition was utilized with variable table speed (*Figure 1*) in order to perform a slower acquisition for the brain (0.4 mm) to generate high count statistics, which enables high-quality reconstruction at the higher matrix required for the brain. The thorax and abdomen, including the pelvis, was acquired at a slightly higher speed of 1 mm/s, which enabled high-quality PET acquisition for standard matrix reconstruction. The acquisition for zone 3, which comprised the thighs, was accelerated at 2.0 mm/s in order to complete the acquisition without time penalty, since the thighs were not very clinically relevant.

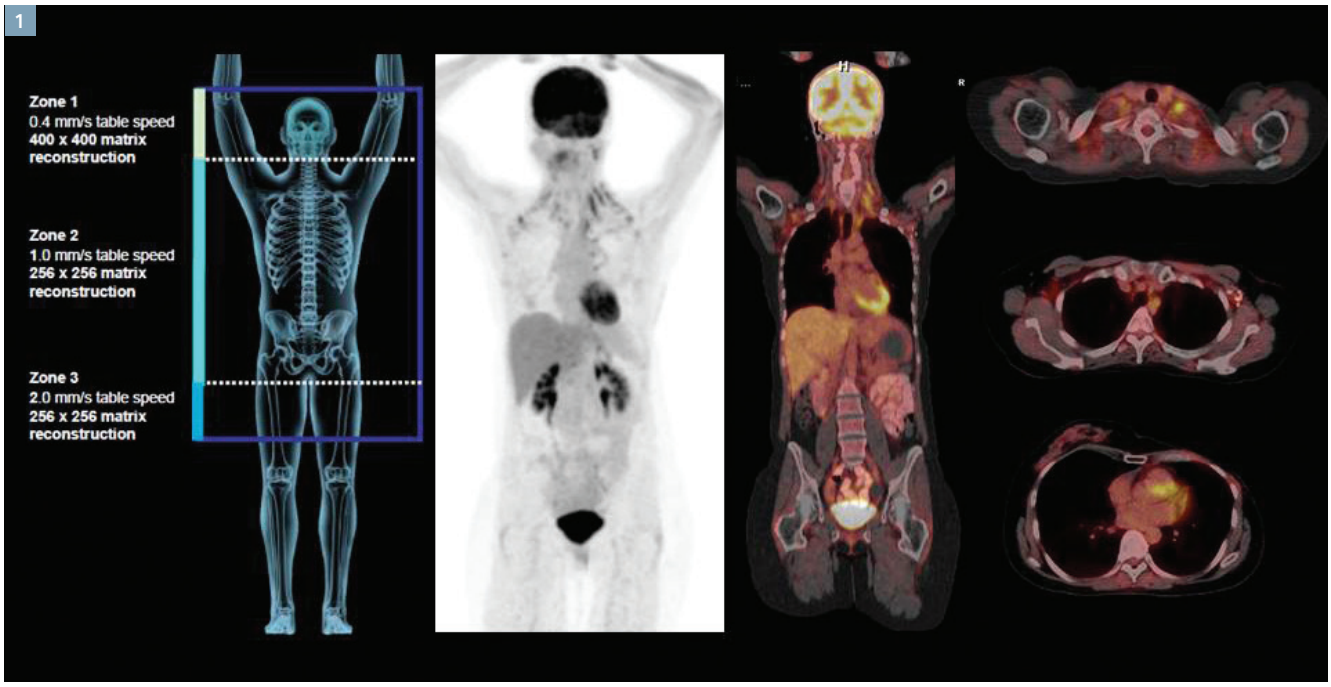

1 The whole-body PET MIP image and the coronal- and axial-fused PET•CT images show significant brown fat but no well-defined metastases, in the body.

Diagnosis

Whole-body PET images show mild non-specific ^{18}F FDG PET•CT uptake in the region of the surgical clips in the left axilla (*Figure 1*) and a significant amount of physiological uptake in brown fat in the bilateral axilla, mediastinum and para-spinal regions of the neck as well as the supraclavicular regions and thorax. There is a large photopenic hypodense lesion in the spleen suggestive of a benign splenic cyst (*Figure 2*). There is also ^{18}F FDG PET•CT uptake in the left para-renal brown fat.

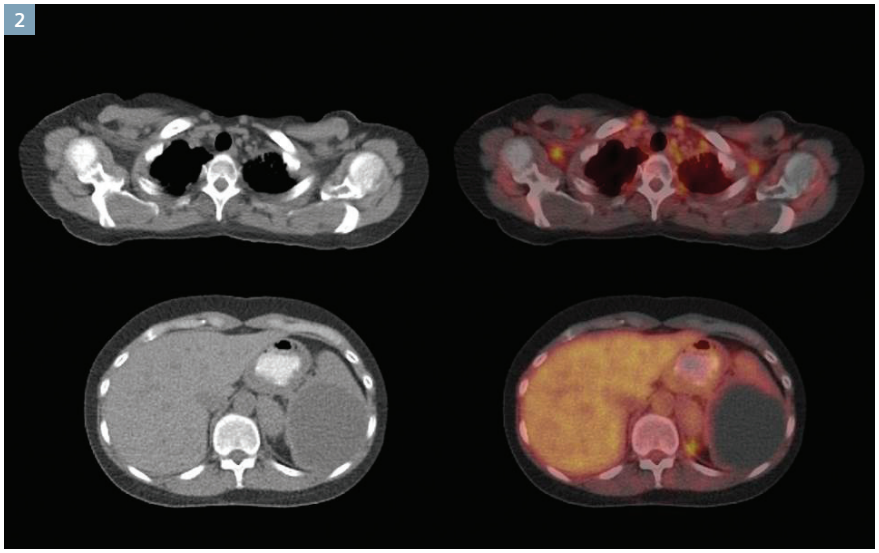

2 CT and fused PET•CT images show brown fat in the neck and photopenic splenic cyst.

3

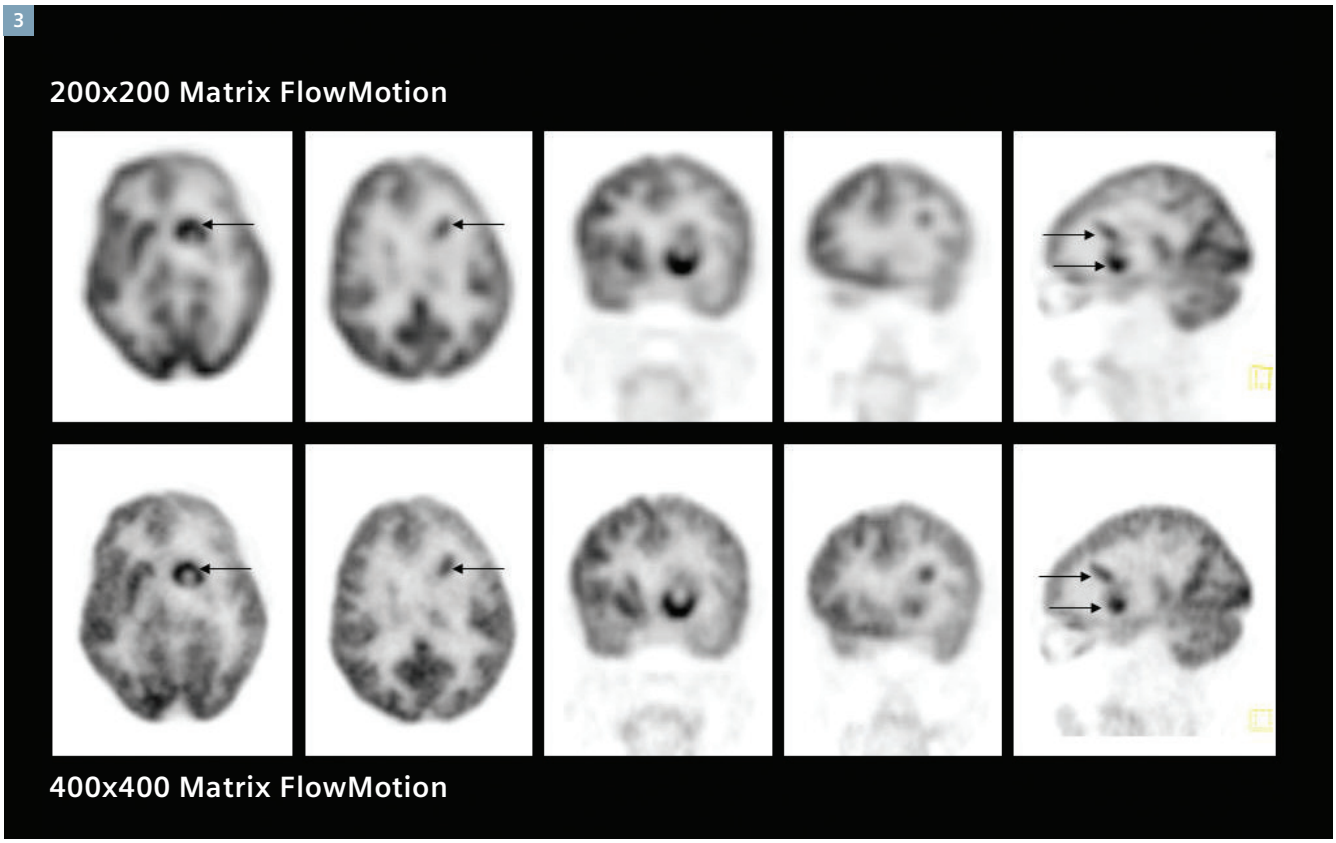

3 Comparison of 200x200 matrix and 400x400 matrix (Hi-Rez) reconstructions of the PET acquisition of the brain shows hypermetabolic metastases in the left basal ganglia.

PET images of the brain demonstrated a hypermetabolic mass in the left basal ganglia that corresponds to the lesion seen on CT, suggestive of brain metastases. The PET brain acquisition was also reconstructed using a 400x400 matrix, due to the higher count statistics enabled by slower table speed acquisition of the brain region, made possible with FlowMotion technology. Higher matrix reconstructions (*Figure 3*) show sharper delineation of the basal ganglial metastases compared to a 200x200 matrix reconstruction. The central necrotic area within the basal ganglial metastases (*arrow*) is more sharply delineated with Hi-Rez reconstruction, along with the delineation of the superior extension of the metastatic lesion (*arrow*). Higher matrix acquisition of the brain requires high count statistics for high reconstruction quality, which is enabled by the slower table speed during the FlowMotion acquisition of the brain.

Careful analysis of Hi-Rez brain PET images also showed relative hypometabolism in the left frontal region and the right cerebellar hemisphere, which is typical of crossed-cerebellar diaschisis (*Figure 4*). Crossed-cerebellar diaschisis is a reversible, matched reduction in blood flow and metabolism in the contralateral cerebellum in patients with supratentorial lesions, including acute cerebral infarction or tumor. This phenomenon is secondary to the interruption of the corticopontocerebellar tract by the lesion, such as the basal ganglial metastases in this case. Higher matrix reconstructions are instrumental for proper demonstration of the mild hypometabolism in the right cerebellar hemisphere.

Comments

In view of the high physiological uptake of FDG in the brain, detection of small brain metastases with PET•CT requires high lesion contrast and higher matrix reconstruction in order to differentiate small hypermetabolic lesions from the surrounding cortex. Higher matrix Hi-Rez reconstruction (400x400 matrix) requires high count statistics in order to generate high-quality reconstructions without excess noise. The slow table speed of 0.4 mm enabled by FlowMotion technology permits such high count statistics acquisition for the brain with unprecendented flexibility, without compromising overall acquisition time, as well as not requiring a separate dedicated brain acquisition.

Value of FlowMotion Technology

This study illustrates the clinical importance of higher matrix reconstruction for improved visualization of brain lesions such as metastases. FlowMotion technology enables very flexible ranges for slow table speed acquisition for higher count statistics, which enables high-quality reconstructions with a 400x400 matrix. This matrix provides for sharper delineation of small intracerebral lesions with higher lesion to background ratio due to lower partial volume effects. In situations where only the brain requires a Hi-Rez reconstruction, FlowMotion enables only the brain to be scanned slowly for higher count statistics with normal or faster scanning for the rest of the body as part of the integrated whole-body PET•CT acquisition. This flexibility ensures patient-specific acquisition for adequate image quality and resolution without undue time penalty.

4

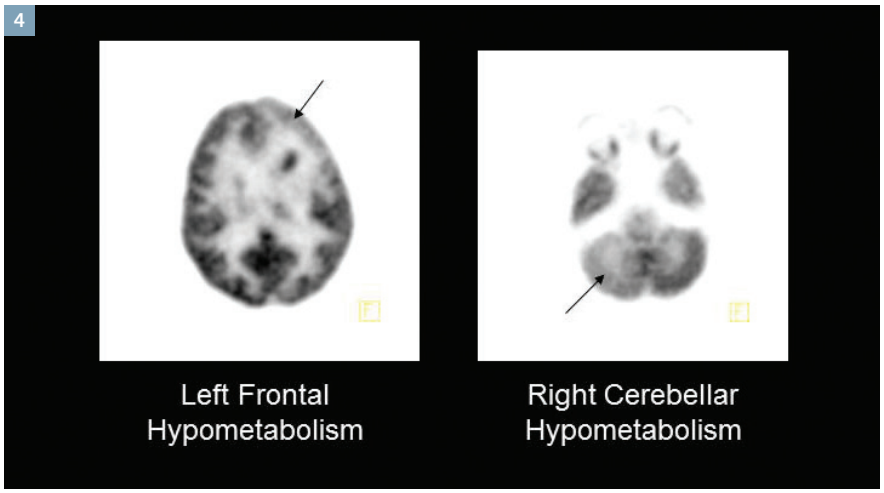

4 Hi-Rez brain PET reconstructions show hypometabolism in the left frontal and right cerebellar hemisphere (i.e., crossed cerebellar diaschisis).

Examination Protocol

Scanner	Biograph mCT Flow™**
Scan dose	8 mCi ^{18}F FDG
CT	100kV 53 eff mAs
PET	FlowMotion variable speed acquisition

* Indications and important safety information on Fludeoxyglucose F 18 injection can be found below. The full prescribing information can be found on pages 49-51.

** Biograph mCT Flow is not commercially available in all countries. Due to regulatory reasons its future availability cannot be guaranteed. Please contact your local Siemens organization for further details.

The statements by Siemens customers described herein are based on results that were achieved in the customer's unique setting. Since there is no "typical" hospital and many variable exist (e.g., hospital size, case mix, level of IT adoption) there can be no guarantee that other customers will achieve the same results.

Indications

Fludeoxyglucose F 18 Injection is indicated for positron emission tomography (PET) imaging in the following settings:

- **Oncology:** For assessment of abnormal glucose metabolism to assist in the evaluation of malignancy in patients with known or suspected abnormalities found by other testing modalities, or in patients with an existing diagnosis of cancer.
- **Cardiology:** For the identification of left ventricular myocardium with residual glucose metabolism and reversible loss of systolic function in patients with coronary artery disease and left ventricular dysfunction, when used together with myocardial perfusion imaging.
- **Neurology:** For the identification of regions of abnormal glucose metabolism associated with foci of epileptic seizures.

Important Safety Information

- **Radiation Risks:** Radiation-emitting products, including Fludeoxyglucose F 18 Injection, may increase the risk for cancer, especially in pediatric patients. Use the smallest dose necessary for imaging and ensure safe handling to protect the patient and health care worker.
- **Blood Glucose Abnormalities:** In the oncology and neurology setting, suboptimal imaging may occur in patients with inadequately regulated blood glucose levels. In these patients, consider medical therapy and laboratory testing to assure at least two days of normoglycemia prior to Fludeoxyglucose F 18 Injection administration.
- **Adverse Reactions:** Hypersensitivity reactions with pruritus, edema and rash have been reported; have emergency resuscitation equipment and personnel immediately available.

Improved Delineation of Pulmonary and Splenic Metastases using FlowMotion Technology with Integrated HD•Chest in a Patient with Lung Carcinoma

By: **Dustin Osborne, PhD, and Yong Bradley, MD, University of Tennessee, Knoxville, TN, USA**

Data courtesy of University of Tennessee, Knoxville, TN, USA

History

An 83-year-old male with a history of peripheral vascular disease, aortic aneurysm, myocardial infarction, hypertension and chronic obstructive pulmonary disease presented with altered mental status. Native CT of the brain showed multiple scattered parenchymal lesions with surrounding edema and mild local mass effect consistent with metastatic disease. CT of the thorax confirmed the diagnosis of Non-Small-Cell Lung Cancer. The patient was referred for PET•CT imaging for primary staging.

A PET•CT scan was performed using FlowMotion™ acquisition with variable table speed an hour after an IV injection of 8 mCi of Fludeoxyglucose F 18* (^{18}F FDG). A 3-zone FlowMotion protocol was used, which applied a table speed of 1.5 mm/s for the head, 0.4 mm/sec in the chest with respiratory gating and 1.5 mm/s for the abdomen, pelvis and extremities. List mode acquisition with respiratory gating was performed throughout the whole-body acquisition with a slower table speed for the thorax to enable integrated reconstruction of HD•Chest images for the thorax. The whole-body data was initially rebuilt as a whole-body 200x200 matrix reconstruction. Subsequently, the same data was reconstructed using the respiratory-gated list mode data with histogramming to define the phases with least motion. The resulting HD•Chest images for the thorax were deemed free of significant respiratory motion. FlowMotion enabled a slower table speed to be used during the chest acquisition, thus ensuring high count statistics and providing high-quality HD•Chest images.

1

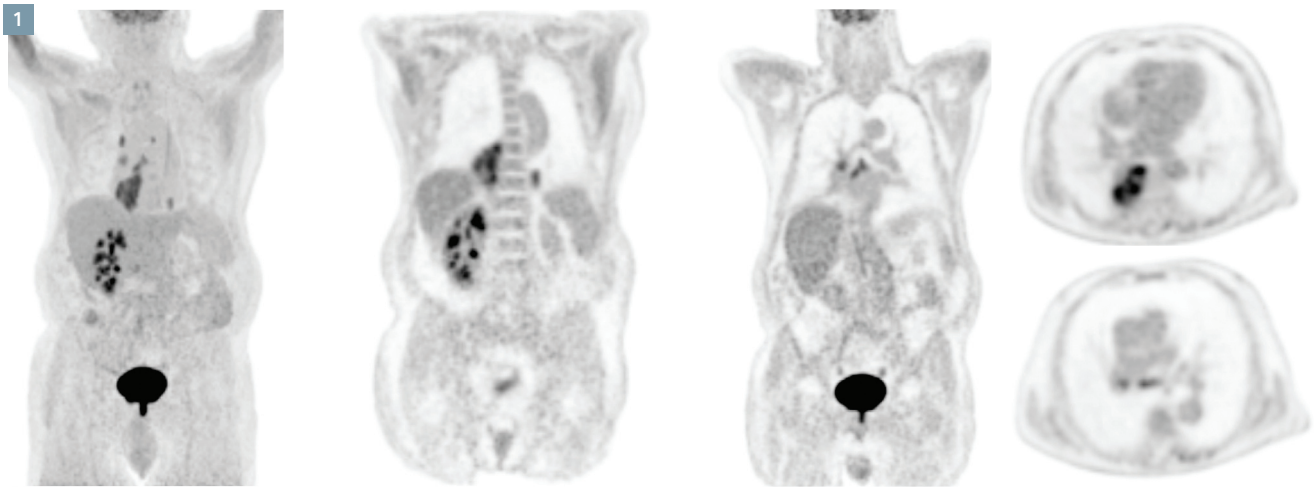

1 A whole-body, non-gated, 200x200 reconstruction of ^{18}F FDG PET data acquired using FlowMotion with variable table speeds.

2A

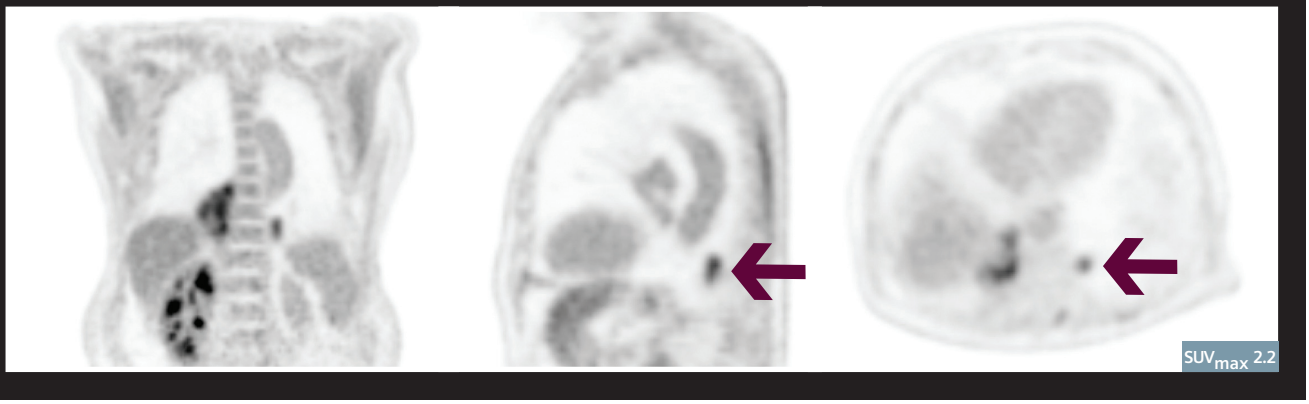

2B

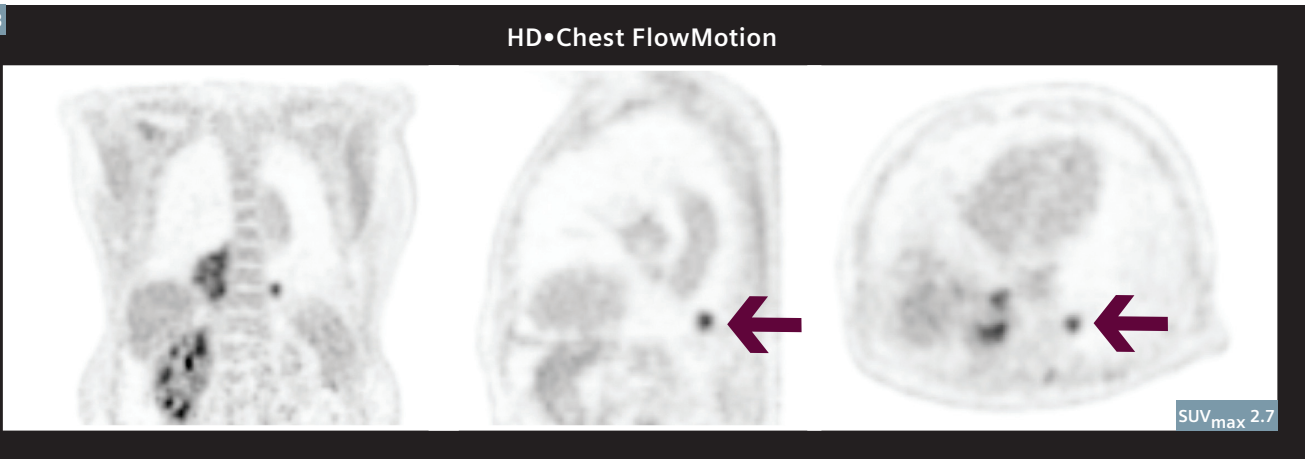

2 When compared to non-gated images *(2A)*, HD•Chest images *(2B)* demonstrated sharper visualization of a hypermetabolic pleural metastatic nodule. The SUV_{max} is significantly increased with HD•Chest.

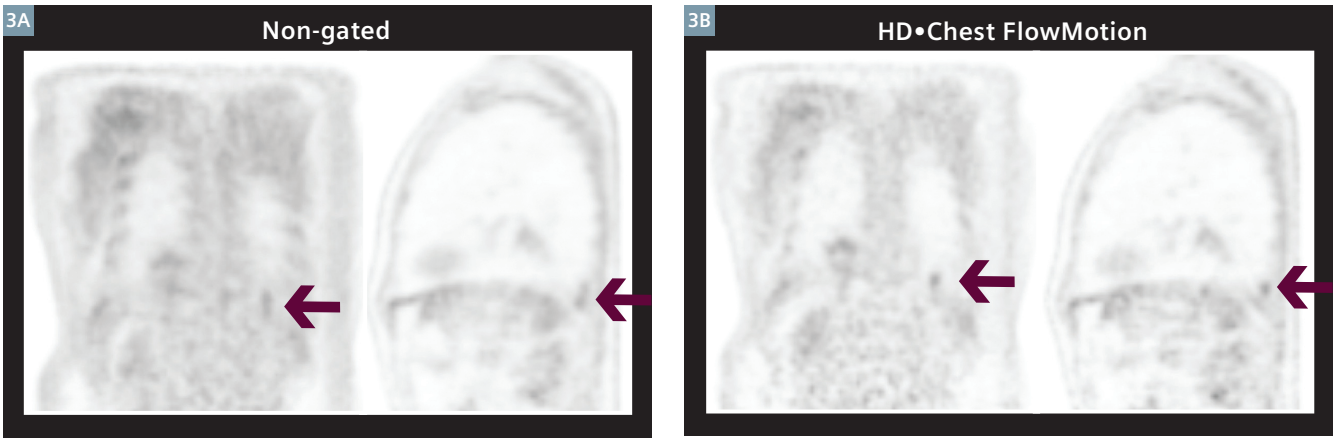

3 A comparison of non-gated *(3A)* and HD•Chest *(3B)* images shows improved definition of another small pleural metastatic deposit using HD•Chest, while the same appears vertically stretched out in the non-gated reconstruction.

Diagnosis

The non-gated study showed a hypermetabolic, posteromedial right lung mass, as well as a small focal hypermetabolic lesion in the medial left lower lobe along with multiple mediastinal lymph node metastases. The pulmonary nodule located in the posterior left lung was identified as having only mildly increased ^{18}F FDG avidity with a max SUV of 2.2 and suffered from significant respiratory motion artifacts measuring approximately 26 mm. There were no significant abdominal, pelvic or skeletal findings except for a large subphrenic space, which appears hypodense on a CT scan that does not show ^{18}F FDG avidity.

HD•Chest images show sharp definition of pleural nodule free of respiratory motion. When SUV_{max} was measured using HD•Chest reconstructed data, all secondary lesions showed at least a 10% increase in SUV_{max} with a maximum increase of 46%. A posterior left lung lesion previously identified as having mild ^{18}F FDG avidity showed a 23% increase in SUV_{max} to 2.7, placing it above common threshold limits and slightly above liver background of 2.4. The respiratory motion artifacts in this lesion were eliminated with the use of HD•Chest, showing the tumor measurement to be only 11 mm. The HD•Chest images also show two areas of focal uptake in the superior portion of the spleen not visible on conventional whole-body PET. These lesions, previously not seen on CT or conventional PET, showed both had SUV_{max} values of approximately 2.4 with measurements of 10 mm and 7 mm respectively.

Comments

PET•CT confirmed a hypermetabolic primary lung mass with multiple metastases in the mediastinal lymph nodes, opposite lung, pleura and spleen. HD•Chest images sharply defined left-lower-lobe metastases in the lung base, as well as pleural and splenic lesions. Improved visualization of such small lesions with motion management contributes to higher accuracy of staging and recurrence detection with PET•CT.

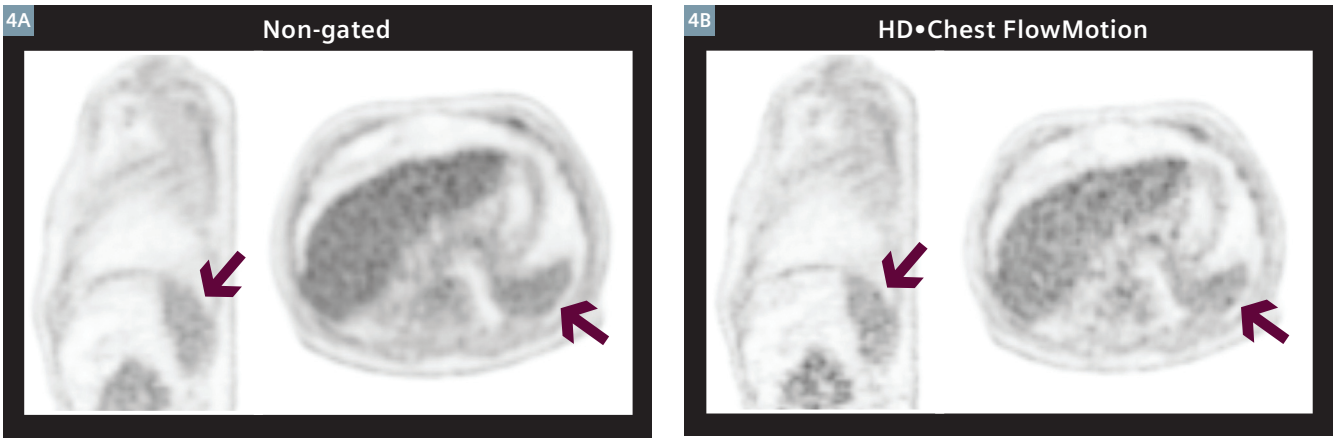

4 With the HD•Chest *(4B)* images, a very small, splenic metastatic deposit with a low level of hypermetabolism above the normal splenic background is visible, while the same lesion is not well delineated on non-gated images *(4A)*.

Value of FlowMotion Technology

HD•Chest reconstruction for the entire thorax with high image quality was made possible by FlowMotion's variable table speed. This enabled respiratory-gated acquisition with high count statistics due to the ability to precisely define a lower table speed for the thorax and upper abdomen. FlowMotion thus enables the integration of respiratory motion-management as an integral part of routine PET imaging.

Examination Protocol

Scanner	Biograph mCT Flow™**
Scan dose	8 mCi (298 MBq/kg) ^{18}F FDG
Scan delay	60 minutes post injection
Parameters	1.5 mm/s; 0.4 mm/s; 1.5 mm/s FlowMotion

* Indications and important safety information on Fludeoxyglucose F 18 injection can be found on page 7. The full prescribing information can be found on pages 49-51.

** Biograph mCT Flow is not commercially available in all countries. Due to regulatory reasons its future availability cannot be guaranteed. Please contact your local Siemens organization for further details.

The statements by Siemens customers described herein are based on results that were achieved in the customer's unique setting. Since there is no "typical" hospital and many variable exist (e.g., hospital size, case mix, level of IT adoption) there can be no guarantee that other customers will achieve the same results.

Radiation Dose Escalation in a Lung Tumor Based on ^{18}F FDG* PET•CT Acquired using FlowMotion with Integrated HD•Chest Motion Management

By: **Dustin Osborne, PhD and Yong Bradley, MD University of Tennessee, Knoxville, TN, USA**

Data courtesy of University of Tennessee, Knoxville, TN, USA

History

A 72-year-old female presented with headaches and respiratory symptoms. MRI and X-ray abnormalities were suggestive of lung cancer. The patient was referred for a Fludeoxyglucose F 18 (^{18}F FDG) PET•CT scan for staging. A whole-body PET•CT scan was performed using FlowMotion™ with respiratory gated acquisition for the thorax and was reconstructed with HD•Chest to eliminate respiratory motion.

Diagnosis

A whole-body PET•CT scan acquired using FlowMotion technology, which enables PET acquisition using continuous table motion, demonstrated a large 6.4 x 4.5 cm necrotic, right-lower-lobe primary mass with an SUV_{max} of 27 with multiple mediastinal lymph node involvement. The image showed only a small necrotic region with a volume of approximately 3 cc.

Comparison of phase-matched respiratory gating to standard non-gated acquisition indicated that the dimensions of the lung mass were more accurately measured with integrated HD•Chest.

The mass measured 5.2 x 4.2 cm on HD•Chest with an SUV_{max} of 30 and multiple lymph involvement. HD•Chest imaging indicated a necrotic core volume of 6.5 cc (a more than two times increase in visualized necrotic core volume).

PET•CT supported confirmation of large primary lung carcinoma with lymph involvement, and the patient was referred for radiation therapy (RT).

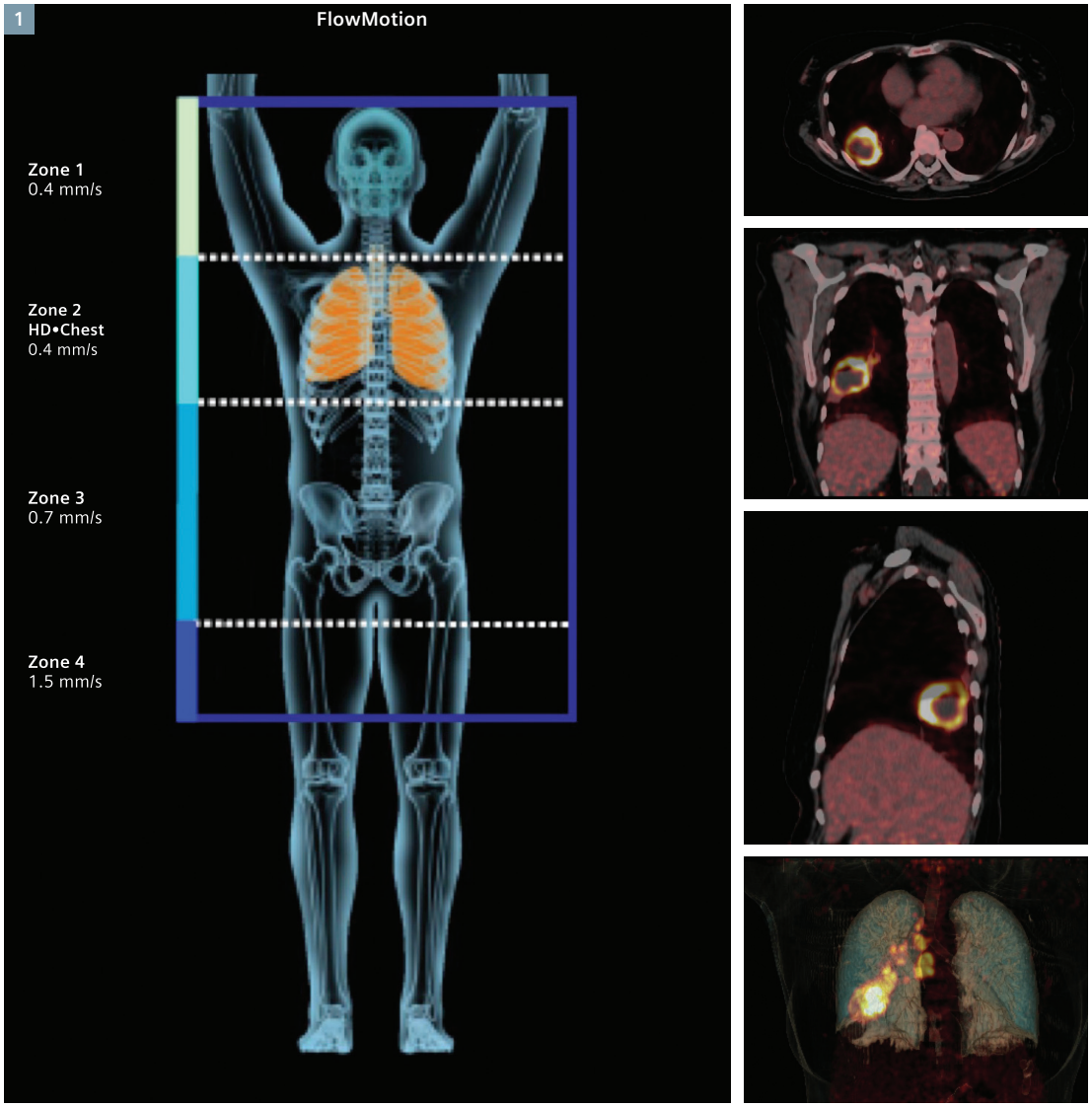

1 HD•Chest image integrated into the whole-body acquisition with FlowMotion technology shows a large lung tumor in the right lower lobe with necrotic center.

2

Standard Radiation Dose Protocol

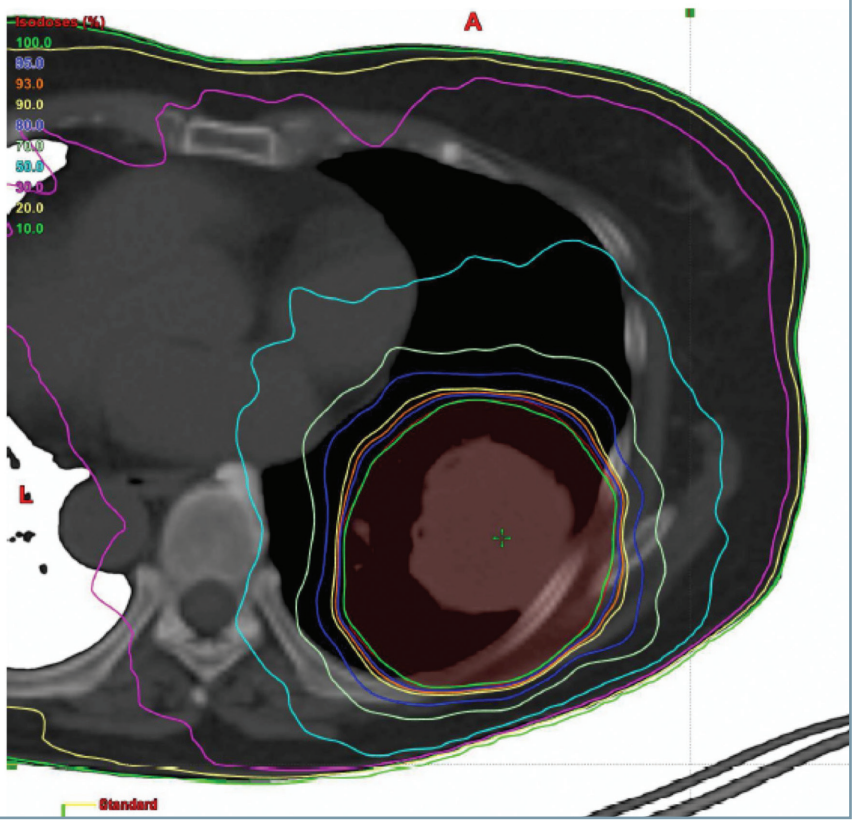

2 Standard conformal radiation therapy (CRT) dose colorwash for the lung tumor based on CT.

3

Dose Escalation Protocol Based on ^{18}F FDG FlowMotion PET•CT with HD•Chest

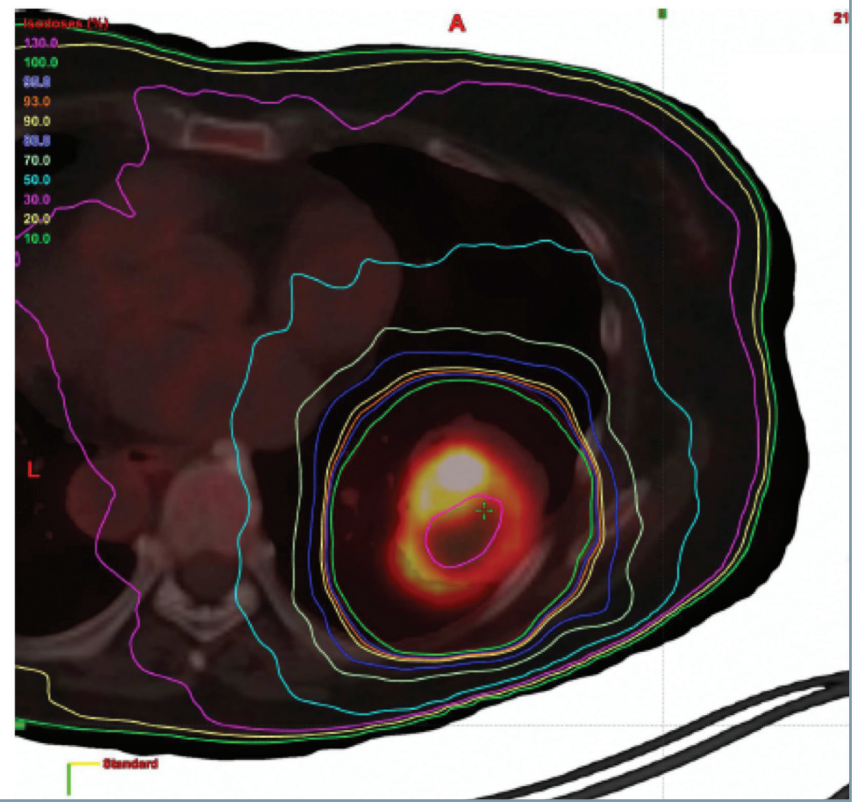

3 RT dose colorwash for same lung lesion with dose escalation strategy aiming to give 130% of dose to the region of the tumor with the highest ^{18}F FDG avidity.

Comments

Radiation Therapy Plan
A typical RT plan includes only 100% of dose given to the tumor volume. For the large primary mass, the initial indicated volume appeared to be small on the conventional whole-body PET/CT. This would have allowed only a standard conformal radiation therapy planning protocol. Because of FlowMotion and its ability to integrate HD•Chest (phase-matched gating) into one, single-routine, whole-body acquisition, the resulting primary lesion was shown to have a much larger necrotic mass, which could benefit from a customized dose painting strategy with dose to the hypoxic region with the highest SUV_{max} levels being increased to approximately 130%.

Therapy Response
Follow-up PET•CT indicated lesion changes consistent with positive therapeutic treatment response. The tumor size was decreased to 4.1 x 3.5 cm with an SUV_{max} of only 4.7 compared to an original SUV_{max} of 30.

This study clearly demonstrates the added value of HD•Chest-based motion management in defining target volumes for RT in lung tumors, especially related to dose escalation strategies. FlowMotion enables precise definition of the range of gated acquisition and makes routine use of HD•Chest possible, which may have an impact on dose escalation approaches for lung tumors, as well as tumors with significant respiratory motion components like liver tumors, pancreatic tumors, etc.

Value of FlowMotion Technology

FlowMotion technology enables variable table speed acquisition, which enables the incorporation of respiratory-gated acquisition within flexible scan ranges. As shown in this case, use of motion management techniques like HD•Chest obtained from respiratory-gated acquisition can improve radiation planning, and the use of FlowMotion enables high use of such techniques, providing high image quality without undue scan-time compromise.

Examination Protocol

Scanner	Biograph mCT Flow™**
Scan dose	10 mCi (370MBq) ^{18}F FDG
Scan delay	90 minutes post injection
FlowMotion acquisition	4-zone protocol with variable table speed with HD•CHEST for thorax

* Indications and important safety information on Fludeoxyglucose F 18 Injection can be found on page 7. The full prescribing information can be found on pages 49-51.

** Biograph mCT Flow is not commercially available in all countries. Due to regulatory reasons its future availability cannot be guaranteed. Please contact your local Siemens organization for further details.

The statements by Siemens customers described herein are based on results that were achieved in the customer's unique setting. Since there is no "typical" hospital and many variable exist (e.g., hospital size, case mix, level of IT adoption) there can be no guarantee that other customers will achieve the same results.

^{82}Rb PET•CT Myocardial Perfusion and Blood Flow Evaluation in a Patient with Multivessel Disease and Impaired Ventricular Function

By: Eric Hong, MD, Consultant Cardiologist

Data courtesy of Parkway Hospitals, Singapore

History

A 61-year-old man with a history of diabetes, hyperlipidemia and hypertension presented with occasional chest discomfort. The patient had a history of myocardial infarction in 1993, which was treated with angioplasty to left anterior descending (LAD) and left circumflex (LCX) arteries. An echocardiography showed left ventricular hypertrophy with normal ejection fraction and anteroseptal wall-motion abnormalities at rest. The patient underwent an ^{82}Rb myocardial perfusion PET•CT study at rest, followed by dipyridamole stress. The study was performed on a Biograph™ mCT PET•CT scanner. A myocardial blood flow (MBF) evaluation was also performed using the *syngo*®.PET Myocardial Blood Flow package.

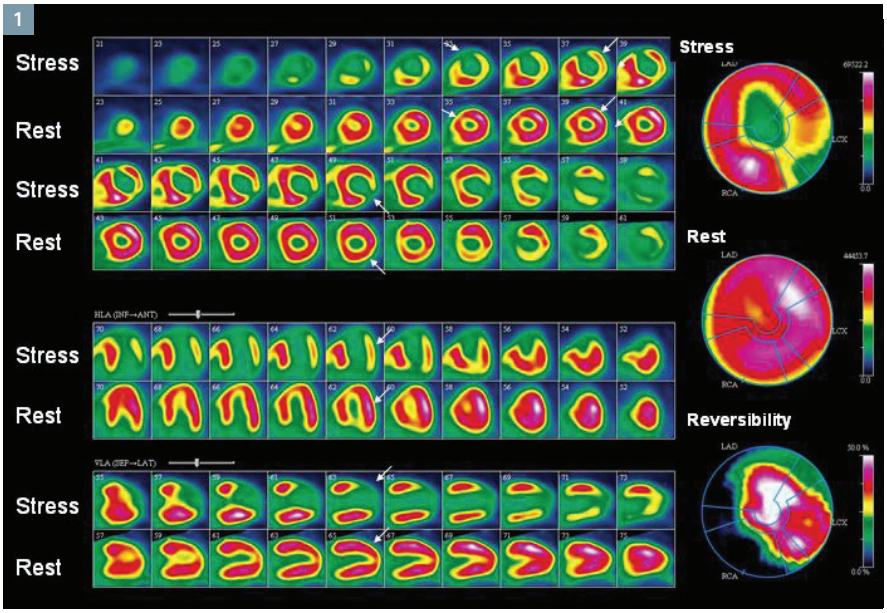

1 Static ^{82}Rb PET myocardial perfusion images show global ischemia with complete reversibility.

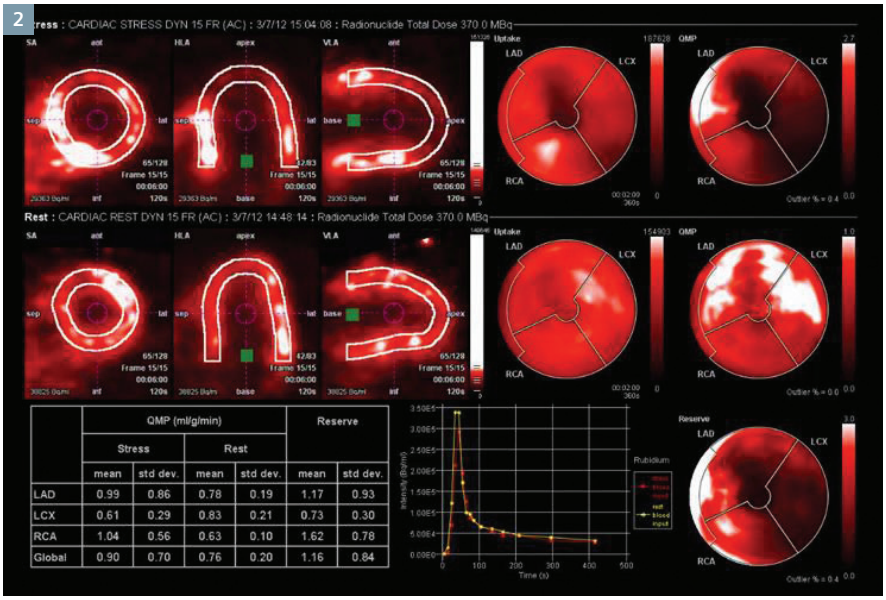

	QMP (ml/g/min)				Reserve	
	Stress		Rest			
	mean	std dev.	mean	std dev.	mean	std dev.
LAD	0.99	0.86	0.78	0.19	1.17	0.93
LCX	0.61	0.29	0.83	0.21	0.73	0.30
RCA	1.04	0.56	0.63	0.10	1.62	0.78
Global	0.90	0.70	0.76	0.20	1.16	0.84

2 MBF evaluation shows severe global decrease in blood flow at peak stress, particularly in the anterior wall, apex and inferolateral wall, along with decreased coronary flow reserve.

Diagnosis

The PET myocardial perfusion study demonstrates severe perfusion defects in the anterior wall, apex and infero-lateral wall. Posterobasal, lateral and inferior walls also show moderate perfusion defects. A rest study shows complete reversibility of all ischemic segments. A small fixed defect in the antero-apical-segment reflects previous myocardial infarction. There is significant post-stress left ventricular (LV) dilatation that normalizes at rest, which is an indicator of multi-vessel disease and stress-induced LV dysfunction.

Coronary flow reserve was severely compromised: Global 1.16, LAD 1.17, LCX 0.73 and right coronary artery (RCA) 1.62. The most severe compromise was in the LCX territory. Stress MBF in the LCX territory was 0.61 ml/gm/min, while the lower limit for normal is accepted to be around 2.0 ml/gm/min.

The patient also had a very high coronary calcium score total: 1704 LM 5, LAD 807, LCX 612 and RCA 280.

Patient was referred for coronary angiography.

A coronary angiography performed in March 2012 demonstrated severe triple vessel disease with serial 95% stenoses in the proximal and mid LAD, as well as 99% stenosis in distal LAD. Proximal and distal LCX arteries showed 95% stenoses. Dominant RCA showed 90% mid-level stenosis and 90% distal stenosis.

The patient underwent successful percutaneous transluminal coronary angioplasty (PTCA) of the diffuse proximal and distal LAD stenosis with 4 overlapping drug eluting stents. Proximal and mid-distal LCX stenoses were also stented. The RCA stenoses were not treated, since intervention was planned for a later date.

The patient underwent a relook coronary angiography after 1 week, which showed patent stents in the proximal-mid LAD, as well as patent stents in the proximal and distal LCX. The calcified diffuse, 90% mid RCA and 90% distal RCA lesions, were successfully stented using drug eluting stents.

Figure 4 shows coronary angiographic images of RCA and LAD, which demonstrate normalization of flow through patent stents in mid and distal RCA as well as in proximal, mid and distal LAD.

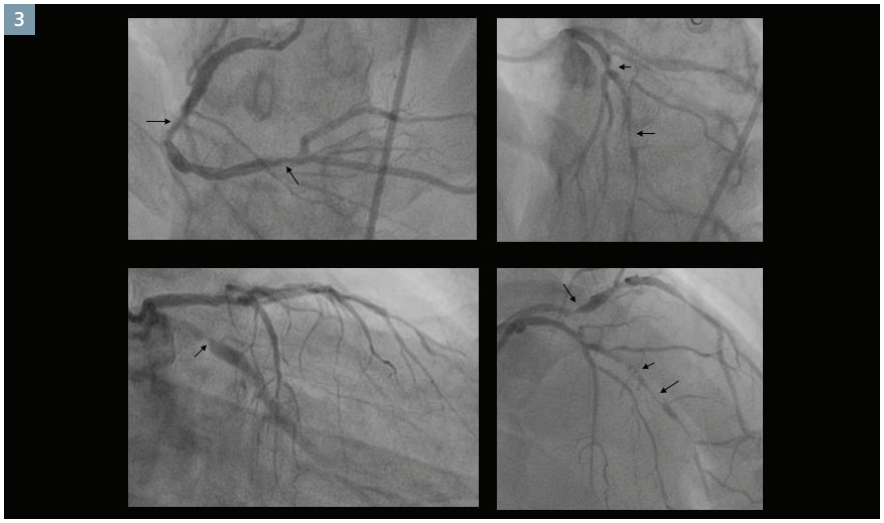

3 Coronary angiography shows multiple stenosis in LAD, RCA and LCX.

4

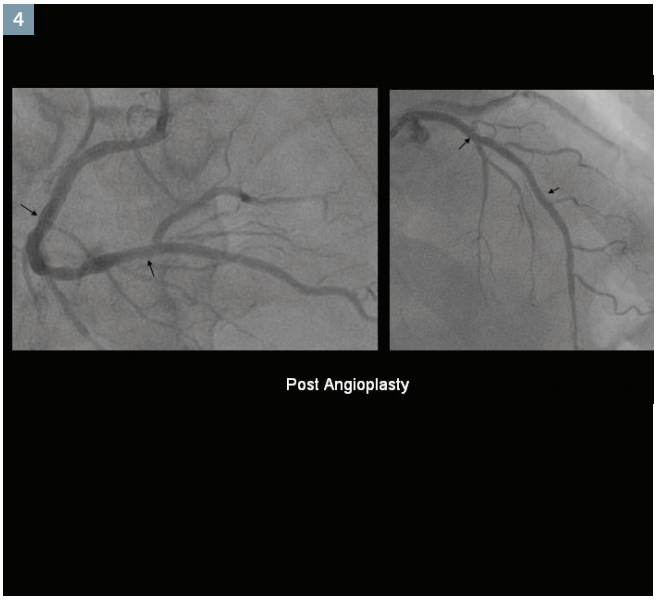

4 Post-stent placement relook coronary angiography showing patent LAD and RCA stents.

5

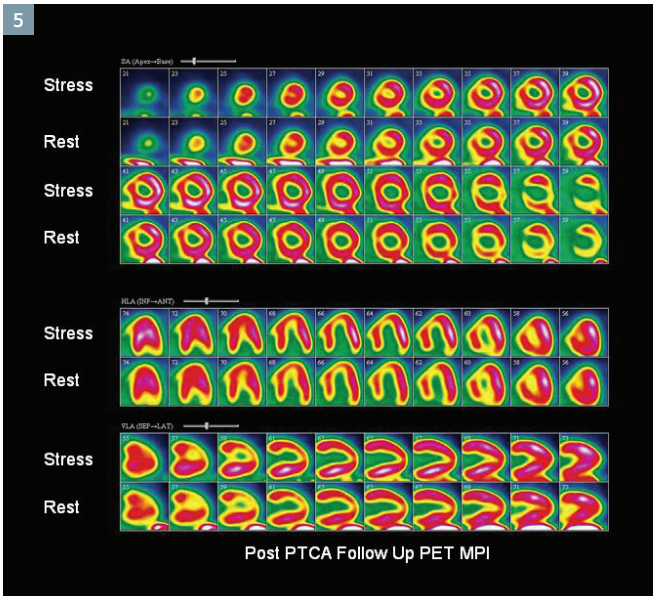

5 Follow-up ^{82}Rb PET myocardial perfusion study shows near normalization of perfusion in most arterial territories.

Subsequently, the patient underwent ^{82}Rb myocardial perfusion PET•CT after 2 months (May 2012) for a post-revascularization follow-up.

The follow-up ^{82}Rb PET stress/rest myocardial perfusion study showed significant improvement of perfusion for all arterial territories with resolution of high-risk features like post-stress LV dilatation. A mild fixed-perfusion defect in the antero-apical segment reflects previous infarction. A small area of residual ischemia was visualized in the inferolateral wall. Left ventricular ejection fraction (LVEF) was calculated to be 49%. Overall, the clinical impression was of significant improvement in global LV perfusion and resolution of high-risk features with minor persistent inferolateral inducible ischemia and moderate LV dysfunction. The patient was put on aggressive medical therapy and close clinical follow-up.

Stress MBF in the LCX territory was 1.89 ml/gm/min, a significant improvement when compared to the pre-PTCA study. The coronary flow reserve was also normal and significantly higher than the previous study: Global 2.32, LAD 2.21, LCX 2.20 and RCA 2.66.

6

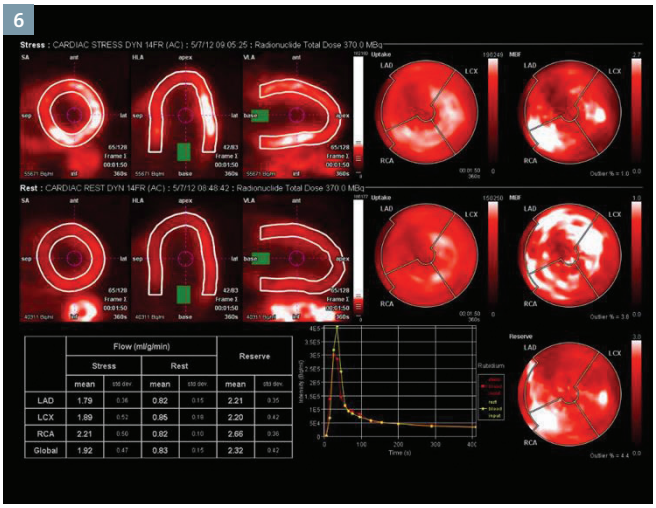

6 Post-PTCA follow-up MBF evaluation shows near normal stress blood flow in all arterial territories.

7

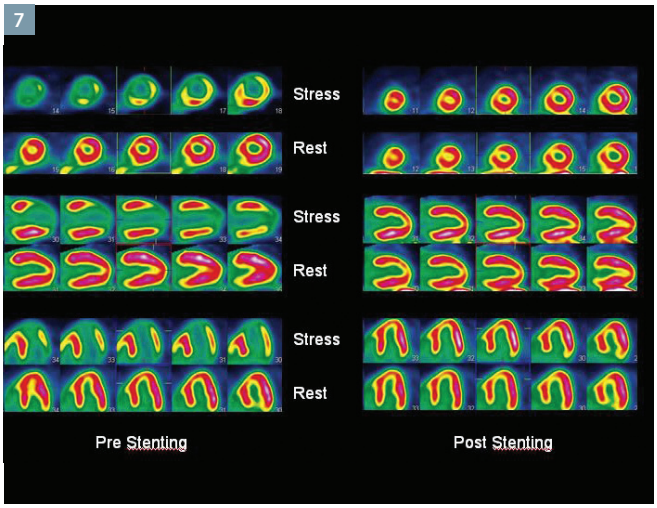

7 Static images of PET myocardial perfusion studies before and after stenting showing significant improvement in perfusion in all arterial territories.

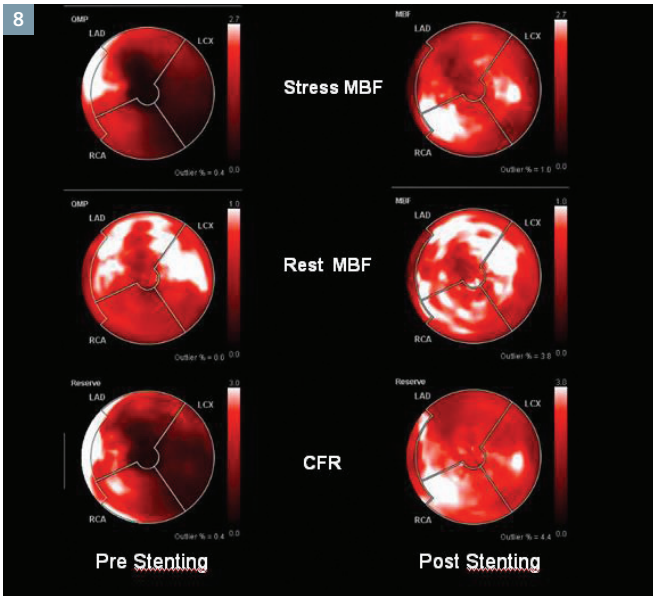

8 Comparison of polar plots in perfusion studies, before and after stenting, demonstrate the extent and severity of ischemia and the near complete resolution of perfusion defect following stenting.

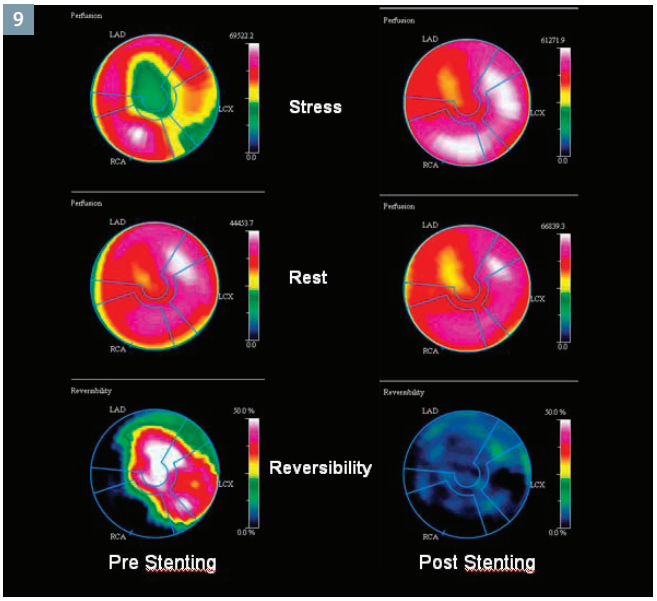

9 Comparison of polar plots of MBF and CFR, before and after stenting, shows the significant improvement in absolute blood flow and flow reserve following stenting.

Comments

This case illustrates the sensitivity of ^{82}Rb PET myocardial perfusion when detecting the extent and severity of ischemia and the extent of reversibility, as well as the accuracy of myocardial blood flow and coronary flow reserve measurements for the evaluation of ischemia severity and as an objective indicator of the success of interventions like stenting. *syngo*.PET MBF software's easy-to-use tool for measuring MBF and CFR is key in the adoption of absolute flow measurements, as a routine, in PET myocardial perfusion, and such an adoption can provide key criteria and benchmarks when measuring therapy response, as in this clinical example.

Value of Technology

Myocardial blood flow measurements using ^{82}Rb dynamic PET perfusion studies are helpful for quantitative assessments of coronary interventions, especially stents. MBF measurements with *syngo*.PET MBF software enable routine usage of such quantitative measurements due to the automated nature of the software and the ease of use.

Examination Protocol

Scanner	Biograph mCT 64
Scan Dose	^{82}Rb 40 mCi injection
Protocols	Acquisition Dynamic List mode (7 min) CT Low dose for CTAC

The statements by Siemens customers described herein are based on results that were achieved in the customer's unique setting. Since there is no "typical" hospital and many variable exist (e.g., hospital size, case mix, level of IT adoption) there can be no guarantee that other customers will achieve the same results.

Sequential PET•CT in a Case of Lymphoma Detecting Post-Chemo-therapy Recurrence

By: **Partha Ghosh, Molecular Imaging Business Unit, Siemens Healthcare**

Data courtesy of Xinhua Hospital, Shanghai, China

History

A 54-year-old male with a clinical and histopathological diagnosis of Hodgkin's Lymphoma was referred for Fludeoxyglucose F 18 (^{18}F FDG)* PET•CT for initial staging (July 2012). The study was performed on a Biograph mCT™ scanner 1 hour following an injection of 10 mCi of ^{18}F FDG. Whole-body acquisition was performed at 2 minutes per bed position. A separate acquisition of the brain and neck was performed with a 5-minute single bed acquisition for higher matrix reconstruction in order to evaluate for cerebral lesions.

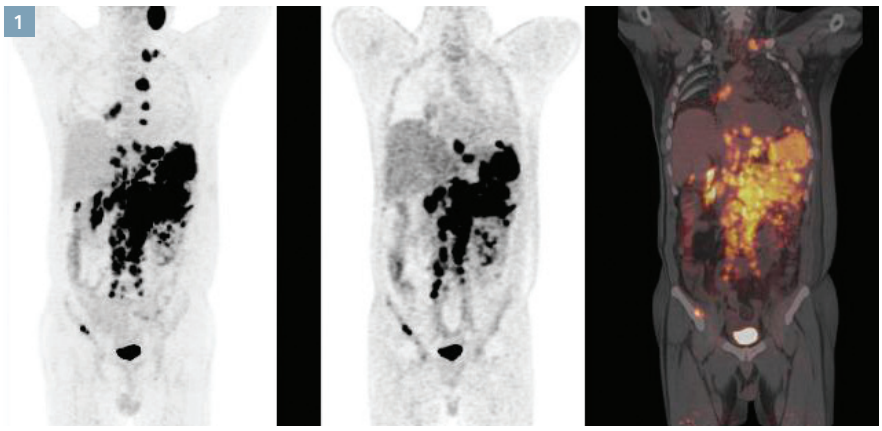

1 MIP, thin MIP of ^{18}F FDG PET and fused PET•CT coronal images of staging PET•CT.

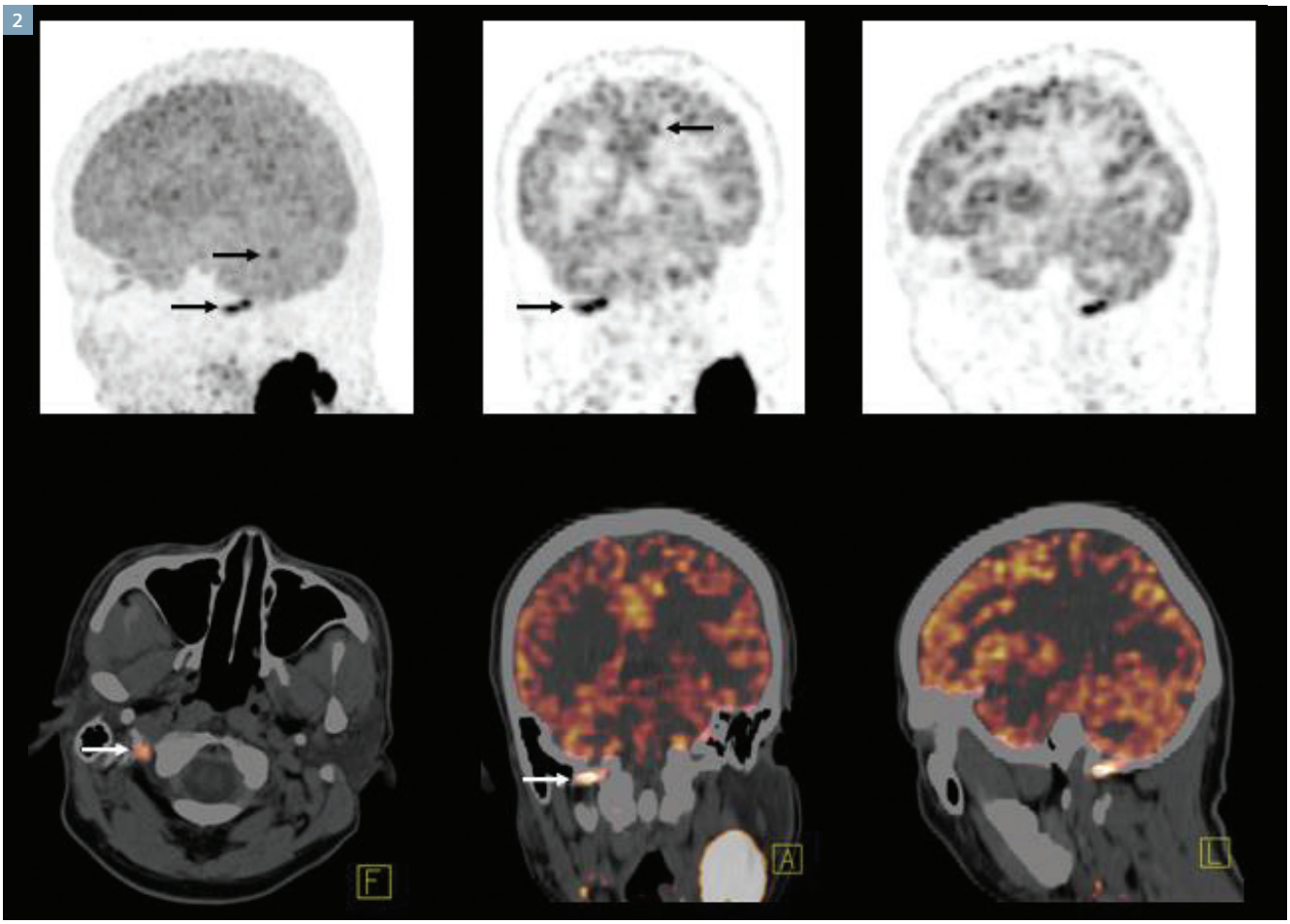

2 High matrix (400x400) reconstruction of brain and neck shows hypermetabolic foci, suggesting involvement of nerve root (*black and white arrows*) and small cortical lesions within the brain (*black arrows*).

Diagnosis

The staging PET•CT study shows extensive matted hypermetabolic lymph nodes in the para-aortic, Iliac, celiac, portal and gastric lymph nodal groups. Also, multiple enlarged hypermetabolic mediastinal nodal groups and left supraclavicular nodes are visible. The focal hypermetabolic region in the pelvis on the right side suggests marrow involvement.

Detection of small lesions within the brain and in the spinal nerve root are enhanced by the Biograph mCT's high lesion contrast—using Time of Flight, PSF reconstruction (ultraHD•PET), and Hi-Rez reconstruction (400x400 matrix), which achieves the finest** volumetric resolution of 95 mm^3.

Because the PET•CT confirmed the advanced stage of lymphoma, the patient was treated with combination chemotherapy (CHOP + Rituximab). Following 2 cycles of chemotherapy, the patient underwent a follow-up ^{18}F FDG PET•CT to evaluate the chemotherapy response.

The ^{18}F FDG PET•CT study performed in September 2012, shows an absence of hypermetabolic nodal lesions throughout the body with considerable regression of the enlarged nodes, suggestive of a remission. The patient completed the regimen of chemotherapy. Clinically, the patient remained disease-free until February 2013, when he was referred for a follow-up ^{18}F FDG PET•CT to assess the status of remission.

PET images show complete resolution of hypermetabolic foci in the study performed on September 2012, after 2 cycles of chemotherapy. However, the follow-up study performed 5 months following chemotherapy in February 2013, shows a small hypermetabolic foci in the right obturator nodes, which was interpreted as a recurrence of lymphoma. No other hypermetabolic lesion visualized in the rest of the body.

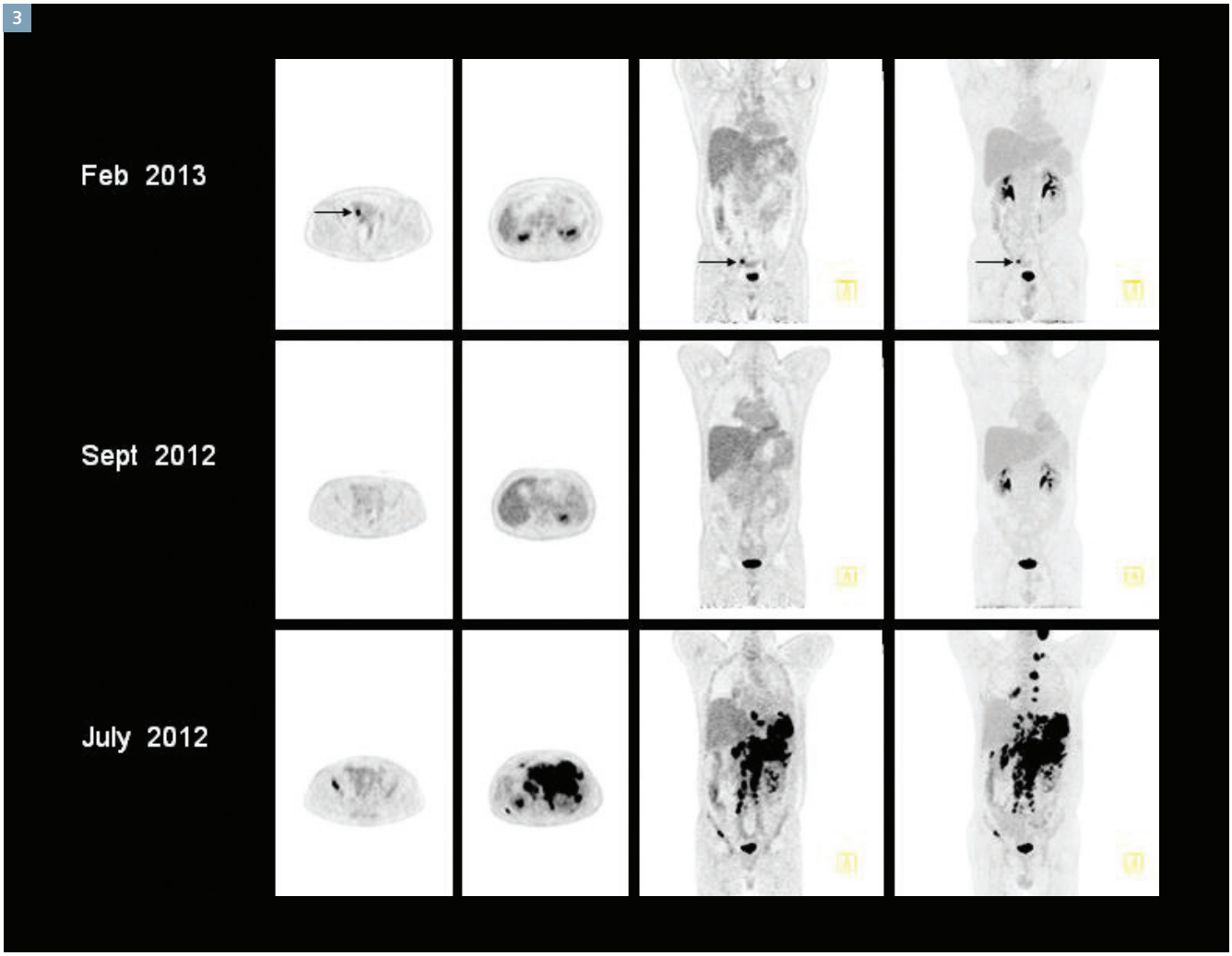

3 PET-only images of three sequential studies demonstrating complete remission after 2 cycles, but small focus of recurrence in the pelvic nodes in the follow-up study.

Comments

Complete resolution of hypermetabolic lymphoma lesions after one or two cycles of chemotherapy, or a significant reduction in the SUV_{max} or SUV_{peak} at mid-therapy PET•CT, is highly predictive of progression-free and overall survival in Hodgkin's and non-Hodgkin's lymphoma (NHL). In patients with newly diagnosed NHL, representative studies have shown disease progression rates of 71%-100% if the mid-treatment PET scan result is regarded as positive, but only 8%-16% with a negative mid-treatment PET scan.[1] Patients with a significant amount of metabolically active disease at mid-treatment PET tend to have a significantly shorter time-to-treatment failure. In patients with NHL, with positive mid-therapy PET, the median times-to-treatment failure was 1.5-10 months, while it was much longer (24-35 months) in patients with negative mid-treatment PET.[2]

However, the patient presented in this example represents a subgroup of people who show relapse even after a negative mid-treatment PET•CT. In a series of 69 patients with diffuse large B cell lymphoma, mid-therapy PET was negative in 51% of the cases; 14% of this group showed relapse within 3 years. But, since 86% of the group with negative mid-therapy PET had 3 years of event-free survival, it reflects positively on the prognostic value of negative mid-therapy PET.[3]

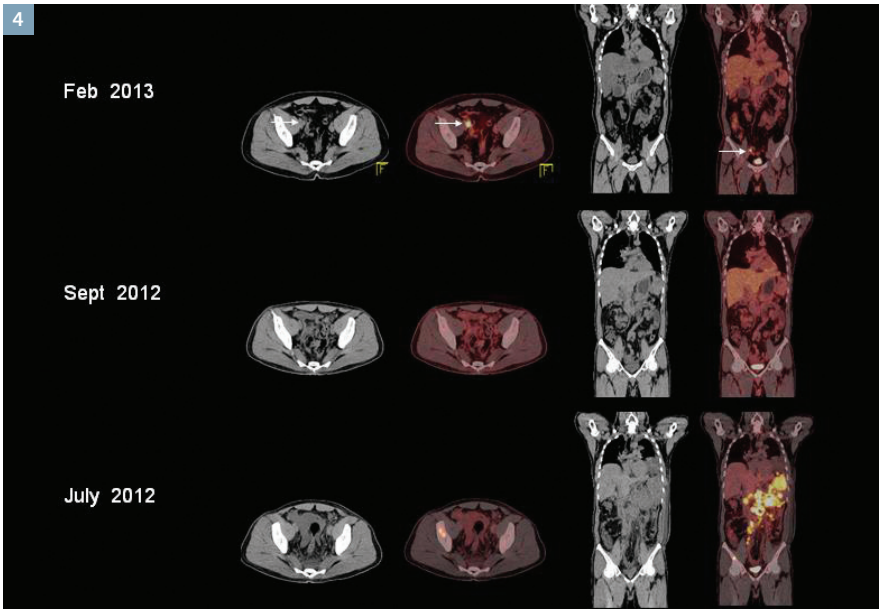

4 Fused PET•CT images show complete resolution of hypermetabolic abdominal and thoracic lymph node mass in the mid-therapy PET•CT study (September 2012). Note the presence of significant residual mass in the para-aortic region without hypermetabolism in the coronal CT and fused images in the mid-therapy study. The follow-up study in February 2013, however, shows small hypermetabolic foci in the pelvis localized to obturator lymph nodes on the right side, suggestive of tumor recurrence. No other lesion visualized.

Value of Technology

Since detection of early recurrence or residual disease is critical to prognostic evaluation and therapeutic decision, the accuracy of PET•CT for detection of small lesions with low levels of hypermetabolism is a key factor in disease management. Technological innovations like high-resolution PET imaging and improved lesion contrast—achieved with time of flight and PSF reconstruction (ultraHD•PET on a Siemens Biograph mCT)—help achieve high diagnostic confidence for detection of small residual or recurrent lymphomatous deposits.

Examination Protocol

Scanner	Biograph mCT
Scan dose	10 mCi ^{18}F FDG
Scan protocol	2 min/bed

* Indications and important safety information on Fludeoxyglucose F 18 injection can be found on page 7. The full prescribing information can be found on pages 49-51.

** Based on volumetric resolution available in competitive literature for systems greater than 70 cm bore size. Data on file.

The statements by Siemens customers described herein are based on results that were achieved in the customer's unique setting. Since there is no "typical" hospital and many variable exist (e.g., hospital size, case mix, level of IT adoption) there can be no guarantee that other customers will achieve the same results.

References:
1 **Kasamon, et al.** *J Nucl Med* 2007; 48:19S–27S.
2 **Mikhaeel et al.** *Ann Oncol.* 2005;16:1514–1523.
3 **Gonzales-Barca** *Nucl Med Commun.* 2013 Jul 22.

Detection of Recurrent Carcinoid Tumor with Ga-68 DOTATATE* PET•CT

By: **Dr. G. Pöpperl, MD**

Data courtesy of Department of Nuclear Medicine, Katharinenhospital Klinikum, Stuttgart, Germany

History

A 60-year-old male with a history of a multifocal carcinoid tumor of the small intestine, treated with surgical resection of intestinal tumor and adjacent bowel loop, along with retroperitoneal lymphadenectomy, presented with progressive diarrhea and hot flashes. Because of the possibility of carcinoid syndrome related to metastatic carcinoid tumor, the patient was referred for PET•CT with Ga-68 DOTATATE, which is a somatostatin analog.

Diagnosis

Fused PET•CT images show focal area of tracer uptake in the area of the surgical anastomosis (*Figure 2, arrow*) performed during previous intestinal resection, which appears to be a local recurrence of the primary carcinoid tumor. Hypermetabolic para-aortic lymph node metastases (*Figure 2, arrows*) and small solitary liver metastases (*Figure 2, arrows*) are also visible.

1 MIP image of Ga-68-DOTATATE-PET showing abdominal and liver metastases. Parenchymal uptake in the liver, spleen, kidneys, bladder and thyroid as well as diffuse uptake in colon wall is within normal limits.

Since the PET•CT findings show intestinal tumor recurrence with para-aortic nodal metastases and liver metastases, which is suggestive of lymphatic and hematogenous spread, the patient was advised to undergo radionuclide therapy with radiolabelled somatostatin analogs, like Lu-177 Octreotate.

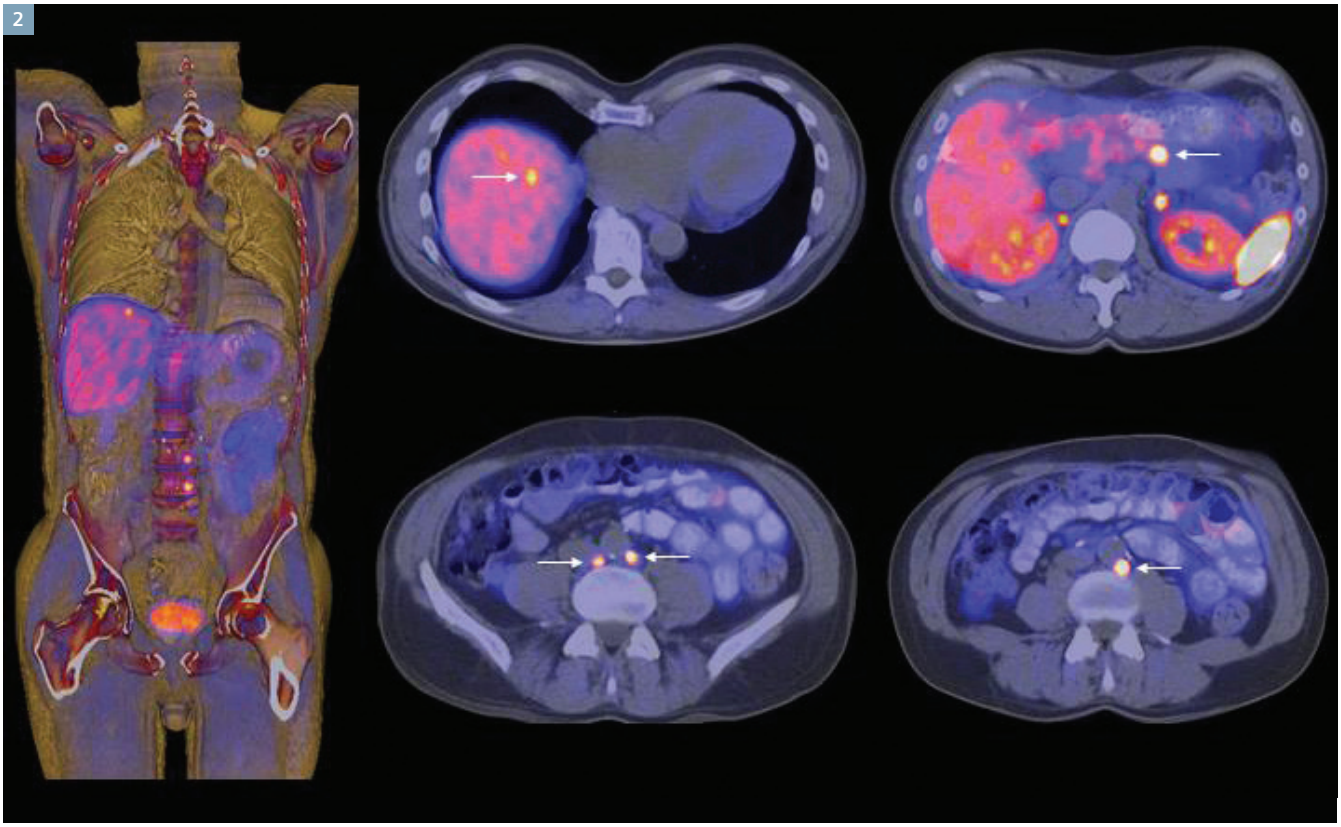

2 Fused PET•CT images show intestinal recurrence and para-aortic and liver metastases.

Comments

In this case, the detection of small liver-lesions is important; it highlights the hematogenous spread of tumors, which is an adverse prognostic indicator. Although In-111-Octreotide-SPECT/CT is the most widely used investigation for detection of metastases from neuroendocrine tumors like carcinoid, Ga-68-DOTATATE-PET/CT has been proven to be more sensitive than SPECT especially in detection of small lesions.[1] This is predominantly due to the higher count statistics generated by PET/CT and attenuation correction. Time-of-flight-PET-acquisition is particularly helpful in detection of small lesions due to the higher lesion-to-background ratio generated.

Value of Technology

High lesion contrast due to time of flight and point spread function (PSF) reconstruction combination (ultraHD•PET), along with high count-rate capability of Biograph™ mCT with TrueV extended field-of-view, was instrumental in the detection of such a small liver-lesion located in the upper edge of the dome of the liver, which was also subject to the maximum respiratory motion. The sharp delineation of such a small liver-lesion within a moving organ at a reasonable acquisition time reflects the count-rate capability and improved lesion-contrast of Biograph mCT.

Examination Protocol

Scanner	Biograph mCT-S(64)
Scan dose	143 MBq Ga-68 DOTATATE
Scan protocol	4 min/bed
CT	130 kV 210 ref mAs
PET	143 MBq Ga-68 DOTATATE, 60 min p.i., 4 min/bed TrueV, ultraHD•PET

* Ga-68 DOTATATE referenced herin is not currently recognized by the US FDA as being safe and effective, and Siemens does not make any claims regarding its use.

The statements by Siemens customers described herein are based on results that were achieved in the customer's unique setting. Since there is no "typical" hospital and many variable exist (e.g., hospital size, case mix, level of IT adoption) there can be no guarantee that other customers will achieve the same results.

Reference:

1 **Buchman et al.,** "Comparison of ^{68}Ga-DOTATOC PET and ^{111}In-DTPAOC (Octreoscan) SPECT in patients with neuroendocrine tumours." *Eur J Nucl Med Mol Imaging.* 2007 Oct; 34(10): 1617-26.

Correlation Between Parameters Derived from ^{18}F FDG* PET•CT and CT Perfusion in Mediastinal Lymph Nodes

By: **Alexander W. Sauter, MD, Maximilian Schulze, MD, and Marius Horger, MD**

Data courtesy of Eberhard Karls University, Tübingen, Germany

History

A 59-year-old man with adenocarcinoma in the left lung underwent PET•CT, performed on a Biograph™ 16 TruePoint PET•CT system, 60 minutes following a 322 MBq Fludeoxyglucose F 18 (^{18}F FDG) injection. The acquisition was initiated with a biphasic, contrast-enhanced CT; this consists of an arterial phase acquisition (thorax) followed by a venous phase acquisition (abdomen and pelvis). For attenuation correction, a low-dose CT scan was used. PET acquisition was performed for 3 minutes per bed position. All values were analyzed using *syngo*® TrueD. Thereafter, the patient underwent a CT perfusion study, using a 128-slice CT system (SOMATOM® Definition AS+). The contrast agent was injected at a flow rate of 5 ml/s. The total acquisition time was 40 seconds. The data evaluation was performed with *syngo* Volume Perfusion CT Body, including the following parameters: tumor blood flow (BF), blood volume (BV) and flow extraction product (K^{trans}).

1

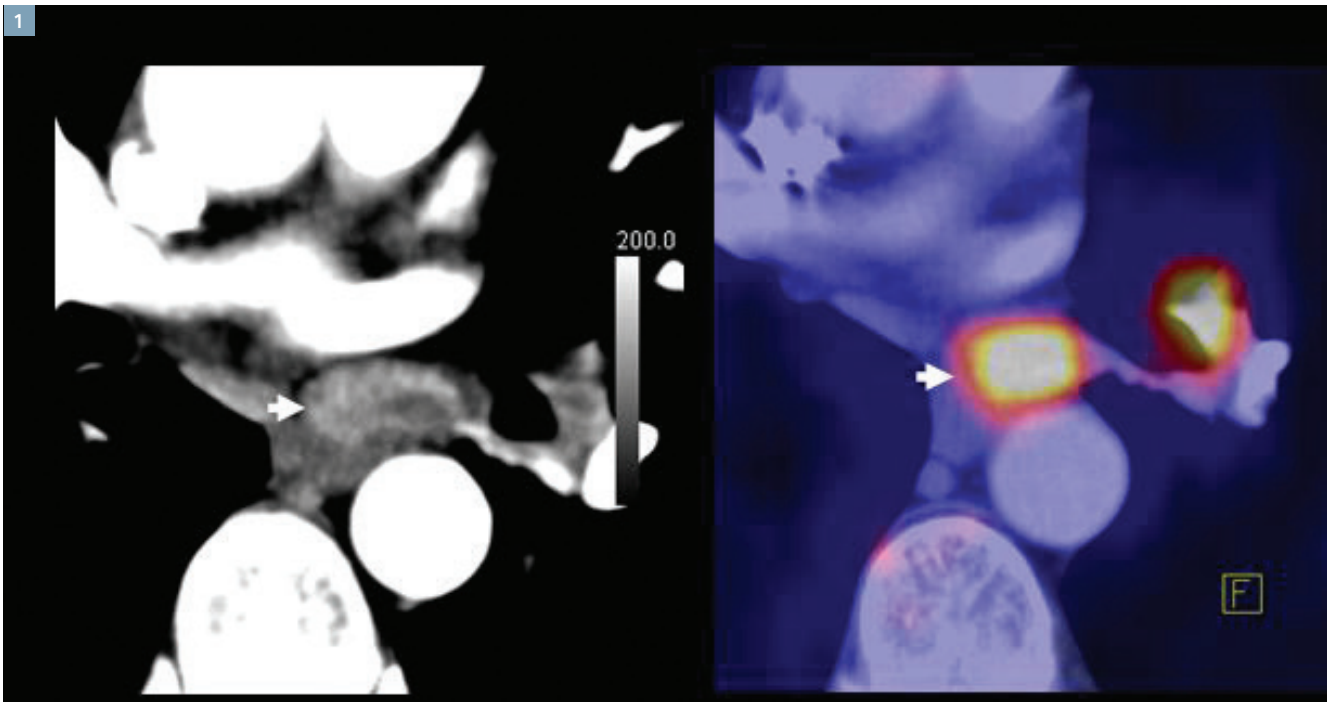

Figure 1a Contrast CT

Figure 1b ^{18}F-FDG PET•CT

1a Contrast CT shows minor enhancement in enlarged subcarinal lymph node mets

1b ^{18}F FDG PET•CT reflects hypermetabolism in subcarinal node

Diagnosis

An arterial phase, contrast-enhanced CT demonstrates enlarged subcarinal (1.5 x 2.9 cm) and hilar lymph nodes with low attenuation (*Figure 1A*). The corresponding ^{18}F FDG PET•CT reflects high uptake in both lymph nodes and a SUV_{avg} value of 6.3 in the subcarinal node (*Figure 1B*).

The perfusion study shows a heterogeneous perfusion with low blood flow (42.52 mL/100 mL/min; *Figure 2A*), blood volume (8.77 mL/100mL; *Figure 2B*) and K^{trans} (33.95 mL/100 mL/min; *Figure 2C*) values in the subcarinal lymph node (*white arrow*). Particularly in the left lower part of the node, these values are potentially very low, presumably reflecting necrosis.

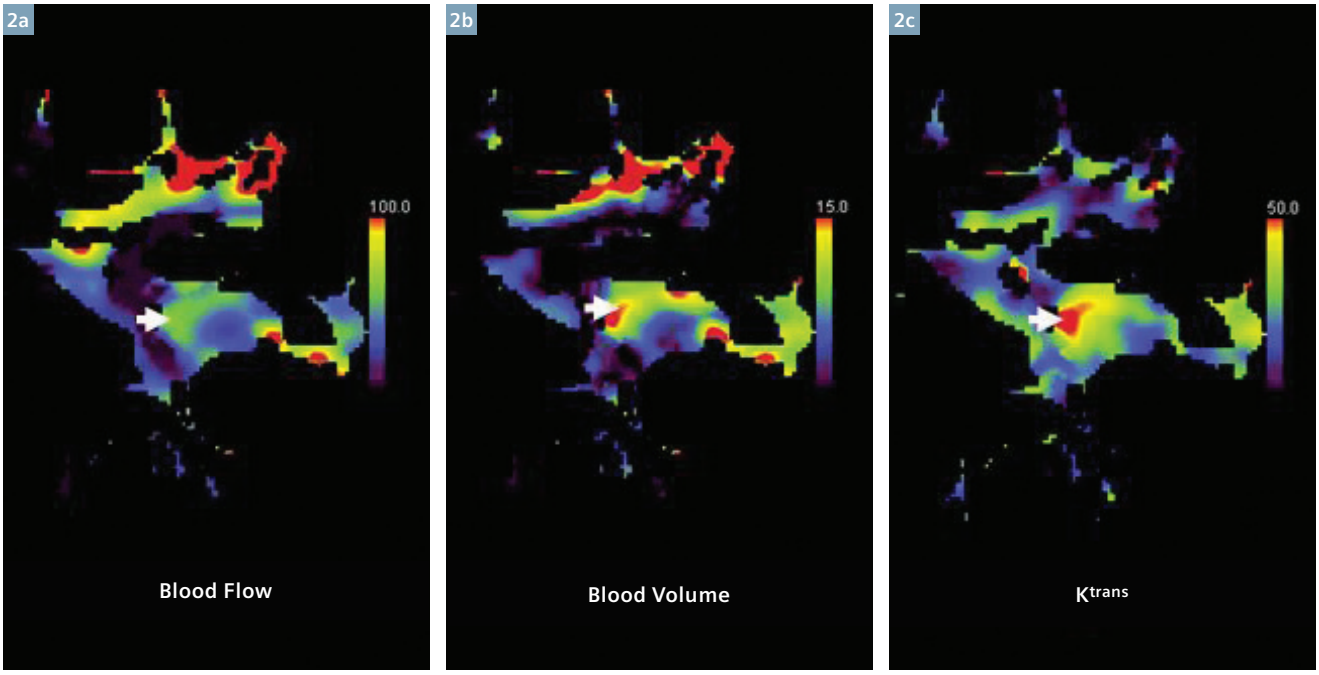

2 2a-c: CT perfusion parametric images reveal low blood flow (*Figure A*), blood volume (*Figure B*) and heterogeneous K^{trans} values (*Figure C*) in subcarinal lymph node metastases.

Comments

This case is one of 17 consecutive patients with non-small cell lung cancer studied with ^{18}F FDG PET•CT and CT perfusion by Sauter et al[1]. No correlations were found between perfusion parameters and ^{18}F FDG uptake for the primary lung tumors.[2] However, in mediastinal lymph nodes, there were negative correlations between BF and SUV_{avg}, BV and SUV_{avg}, and BV and SUV_{max}.[2] No correlations could be documented for BF and SUV_{max}, K^{trans} and SUV_{avg}, or K^{trans} and SUV_{max}. In lymph node metastasis, an inverse correlation between perfusion and glucose metabolism seems to be present.

This inverse correlation may be related to hypoxia in mediastinal lymph nodes, which may enhance radiation resistance and hypermetabolism. On the other hand, inflammatory lung diseases, such as lung abscess, can cause reactive lymph node enlargements and an increase in perfusion values. Such reactive nodes are often present in patients with lung tumors, secondary to inflammatory conditions unrelated to the tumor. Differentiation between malignant and reactive lymph nodes is a problem with ^{18}F FDG PET•CT since both may show increased glucose metabolism. CT perfusion might be helpful in differentiation between metastatic and inflammatory lymph nodes. Since ^{18}F FDG PET•CT shows hypermetabolism in both malignant nodes and nodes with reactive hyperplasia secondary to infection or inflammation, use of CT perfusion as part of an integrated study may help advance lesion characterization with ^{18}F FDG PET•CT.

Value of Technology

Biograph combines CT perfusion capabilities with high temporal resolution, along with high resolution PET imaging for sharp delineation of primary tumor margins as well as small lymph nodal lesions. This combination of CT Perfusion and PET with high resolution and quantitative accuracy provides improved characterization of lymph node lesions, as this case study demonstrates.

Examination Protocol

Scanner	Biograph TruePoint 16
Scan dose	334 MBq ^{18}F FDG
Scan protocol	3 min/bed PET acquisition

* Indications and important safety information on Fludeoxyglucose F 18 injection can be found on page 7. The full prescribing information can be found on pages 49-51.

The statements by Siemens customers described herein are based on results that were achieved in the customer's unique setting. Since there is no "typical" hospital and many variable exist (e.g., hospital size, case mix, level of IT adoption) there can be no guarantee that other customers will achieve the same results.

References:

1 **Sauter AW, Winterstein S, Spira D, Hetzel J, Schulze M, Mueller M, Pfannenberg C, Claussen CD, Klotz E, Hann von Weyhern C, Horger MS.** Multifunctional profiling of non-small cell lung cancer using ^{18}F-FDG PET/CT and volume perfusion CT. *J Nucl Med.* 2012 Apr;53(4):521-9.

2. **Sauter AW, Spira D, Schulze M, Pfannenberg C, Hetzel J, Reimold M, Klotz E, Claussen CD** *Eur J Nucl Med Mol Imaging.* 2013 May;40(5):677-84. doi: 10.1007/s00259-012-2318-2. Epub 2013 Jan 10. Correlation between [^{18}F]FDG PET/CT and volume perfusion CT in primary tumours and mediastinal lymph nodes of non-small-cell lung cancer.

Delineation of Femoral Marrow Infiltration in a Patient of Lymphoma Using xSPECT Bone and CT

By: **Partha Ghosh, MD, Molecular Imaging Business Unit, Siemens Healthcare**

Data courtesy of The Johns Hopkins Hospital, Baltimore, MD, USA

History

A 72-year-old man with a history of non-Hodgkin's lymphoma treated with chemotherapy underwent a ^{99m}Tc MDP bone scan to evaluate osseous lesions. A recently performed MRI of the pelvis showed slight hyperintensity in the right femoral neck in the fat-suppressed images, which was suspicious of marrow infiltration.

An xSPECT* study was performed three hours following IV injection of 27.4 mCi ^{99m}Tc MDP. Initial planar images were followed by xSPECT acquisition. 3D iterative reconstruction and xSPECT Bone* reconstructions were performed for comparison.

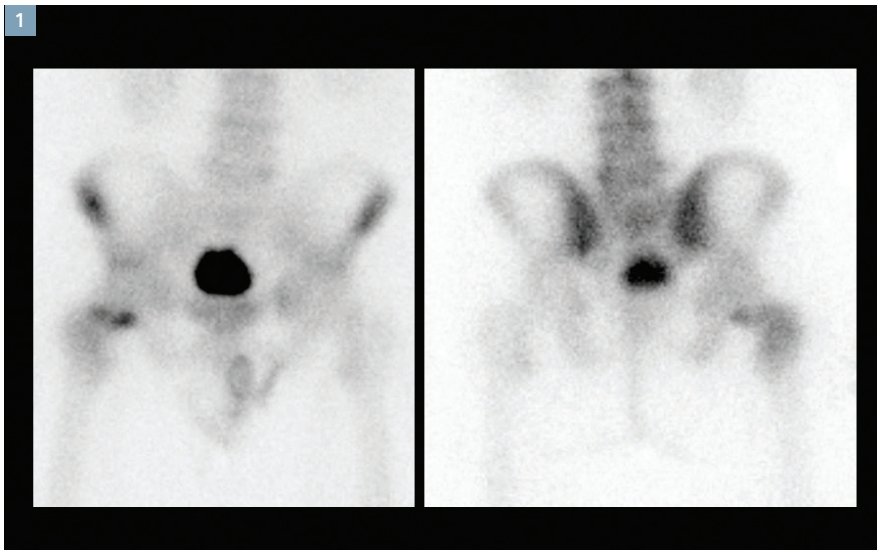

1 Anterior (*left*) and posterior (*right*) planar images of the pelvis show focal increase in uptake in the right femoral neck, especially towards the medial end.

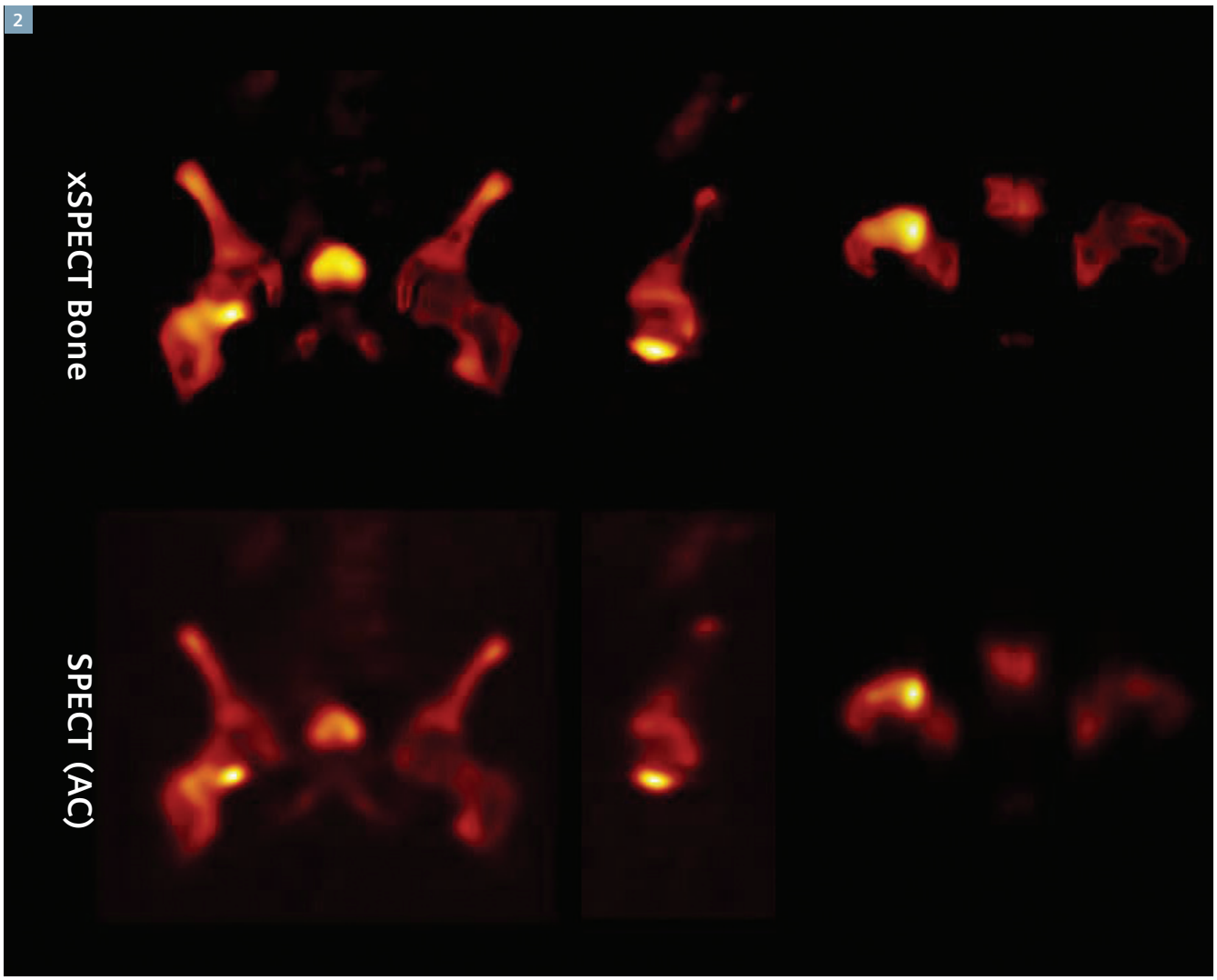

2 Comparison of xSPECT Bone and SPECT (AC) reconstruction of the pelvis demonstrate sharp delineation of the focal hot area in the femoral neck.

Diagnosis

xSPECT Bone sharply defines the focal area of increased uptake in the medial margin of the neck of the femur adjacent to the femoral head. The rest of the femoral neck and the intertrochanteric crest also shows slightly increased uptake. The femoral head uptake appears normal. Compared to SPECT (AC), the xSPECT Bone images show sharper margins of the hypermetabolic foci in the femoral neck as well as sharper delineation of the femoral head, trochanteric regions, intertrochanteric crest and the rest of the pelvis and acetabulum.

CT shows mild sclerosis involving the femoral neck just adjacent to the femoral head, predominantly in the anterior and inferior aspect of the neck. Fusion of CT with xSPECT Bone shows exact coregistration of the focal increase in uptake with the zone of sclerosis. The correlation of the focal area of skeletal hypermetabolism, along with the associated sclerosis seen on CT in view of the MRI findings at the same area, strongly suggest the presence of lymphomatous infiltration in the marrow of the femoral neck.

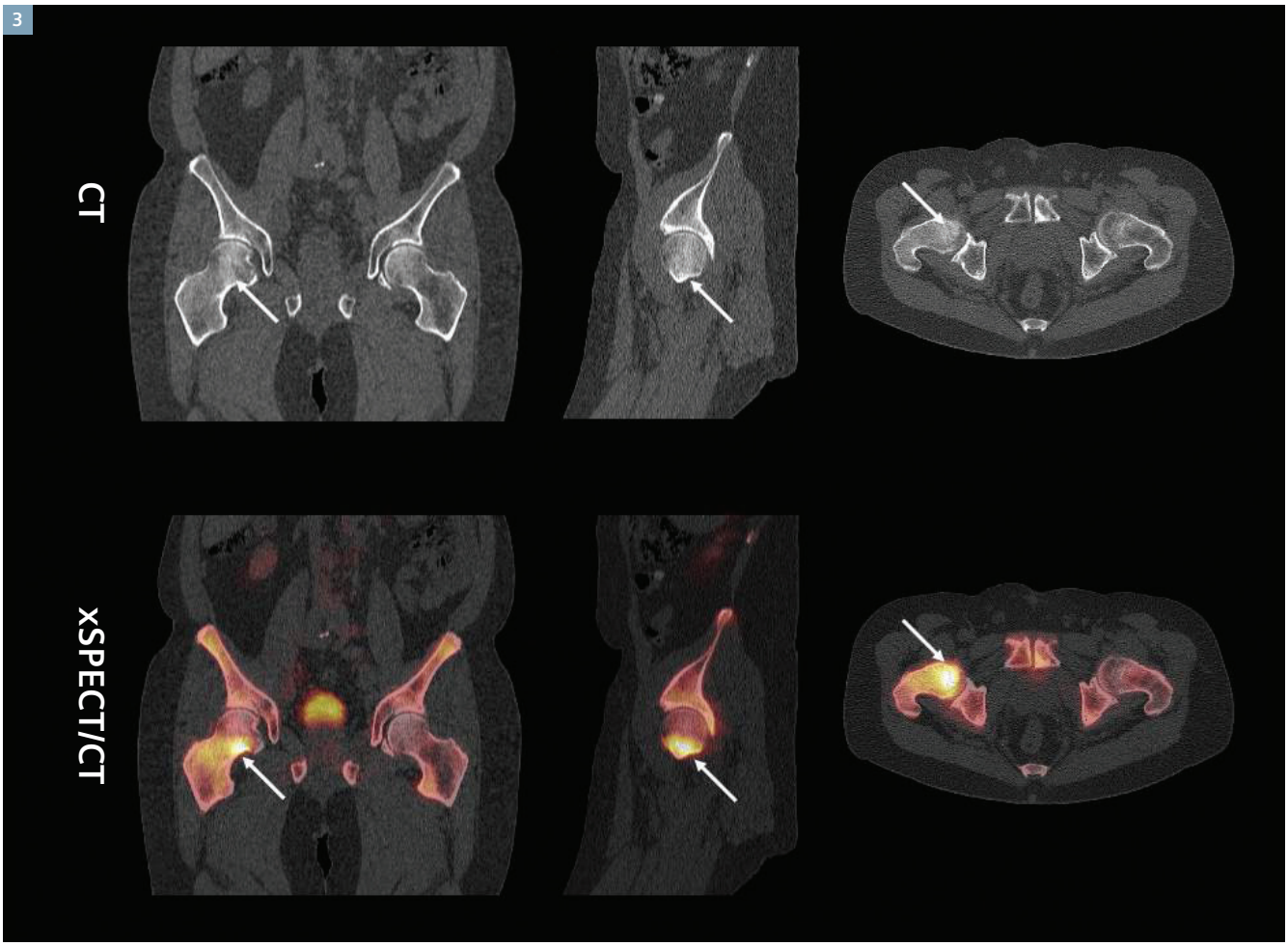

3 CT and fusion of CT and xSPECT Bone show mild sclerosis in the femoral neck, which corresponds to the focal area of increased uptake in the medial margin of the femoral neck.

Comments

Marrow infiltration is common in advanced lymphoma. PET/CT and MRI are both highly sensitive for detection of marrow infiltration.[1] In this clinical example, the MRI findings were suspicious of marrow involvement, but the xSPECT Bone and CT information was supportive of the final diagnosis of lymphomatous infiltration of the femoral neck marrow. The increased sclerosis seen on CT along with the skeletal hypermetabolism may be related to osteoblastic activity stimulated by the infiltrating lymphoma cells.

Value of xSPECT Bone Technology

xSPECT Bone sharply defines the extent of marrow infiltration in the femoral neck by lymphoma and correlates it with the degree and extent of sclerosis seen on CT. The well-defined boundaries of the skeletal hypermetabolism defined by xSPECT Bone provides information about the degree of involvement of the marrow of the greater trochanter and upper part of the femoral shaft beyond the heavily infiltrated region in the lower part of the femoral neck, thereby illustrating the greater extent of lymphomatous infiltration than was estimated from the CT or SPECT only.

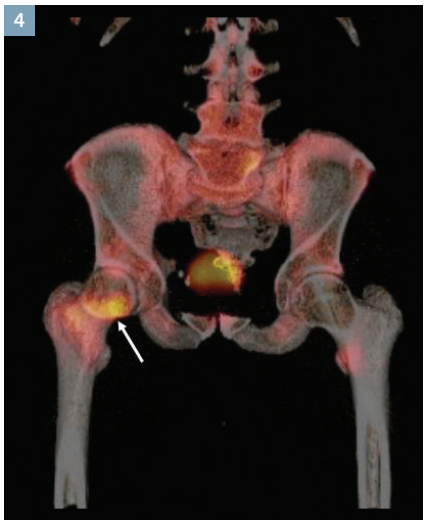

4 Volume rendering of the fusion of CT and xSPECT Bone shows the focal increase in uptake involving the anterior and inferior part of the junction of the femoral head and the neck with most increase in the inferomedial part.

Examination Protocol

Scanner	Symbia Intevo*™
Scan dose	27.4 mCi ^{99m}Tc MDP IV injection
Scan protocol	3 hour post-injection delay
SPECT	32 frames, 30 seconds/frame
CT	130kV 31 eff mAs, 2 mm slice thickness, 16x1.25 mm collimation

* Symbia Intevo, xSPECT and xSPECT Bone are not commercially available in all countries. Due to regulatory reasons their future availability cannot be guaranteed. Please contact your local Siemens organization for further details.

The statements by Siemens customers described herein are based on results that were achieved in the customer's unique setting. Since there is no "typical" hospital and many variable exist (e.g., hospital size, case mix, level of IT adoption) there can be no guarantee that other customers will achieve the same results.

Reference:
1 **Wu, et al.,** 2012, *Eur J Radiol.*, Feb; 81(2):303-11.

Detection of Skeletal Metastases with xSPECT Bone

By: **Zsolt Szabo, MD, PhD, Professor, Department of Radiology, Johns Hopkins Medicine, Baltimore, MD, USA**

Data courtesy of The Johns Hopkins Hospital, Baltimore, MD, USA

History

A 50-year-old man presented with untreated prostate cancer and progressively increasing PSA (PSA increasing from 11 to 233 within 4 years). A ^{99m}Tc MDP bone scan was performed to evaluate for skeletal metastases.

Diagnosis

The planar study demonstrated increased uptake in the right sacroiliac joint, which appeared to be related to degenerative changes, but given the patient's PSA levels, was considered suspicious. Mild degenerative disease in the bilateral acromioclavicular joints, sternoclavicular joints, patellofemoral joints, tibial tuberosities as well as lumbar vertebrae were also visualized. No other well-defined focal area of increased uptake suggestive of skeletal metastases was seen.

In view of the suspicious nature of the sacroiliac joint uptake, a dedicated xSPECT* (full integration of SPECT and CT) acquisition of the pelvis was performed with integrated thin-slice CT.

Comparison images of standard 3D Iterative Reconstruction of bone SPECT and xSPECT Bone* images at a slice through the sacroiliac joint show a small focal hypermetabolic area on the dorsal aspect of the ileum adjacent to the right sacroiliac joint. When compared to SPECT with attenuation correction (AC), the xSPECT Bone images show sharp definition of the hypermetabolic lesion with clear distinction of the lesion location from the adjacent sacroiliac joint margin. With SPECT (AC), the lesion appears larger and ill-defined, and no distinction of the lesion location from the sacroiliac joint is possible.

CT (*Figure 4*) demonstrates a small focal area of of sclerosis in the ileum adjacent to but distinct from the right sacroiliac joint space, which corresponds exactly to the focal hot area seen on the corresponding slices on xSPECT Bone. xSPECT also sharply defines the right sacroiliac joint margin thereby clearly differentiating the focal hot iliac bone lesion from the sacroiliac joint. The sharp definition of the focal bone lesion when compared to the minor sclerosis seen in the corresponding CT slices illustrates enhanced lesion margin resolution achieved by xSPECT.

1

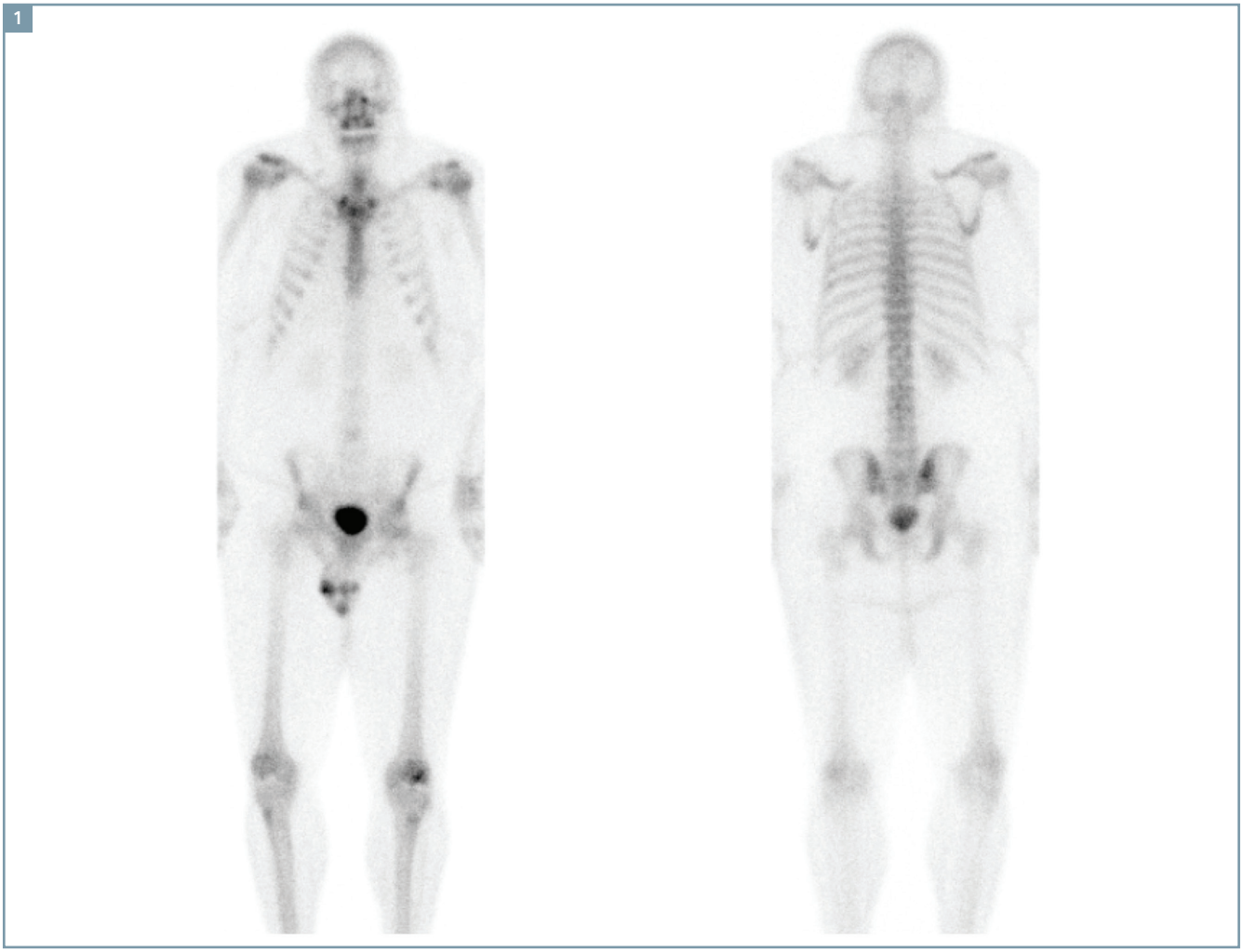

1 ^{99m}Tc MDP planar bone study.

2

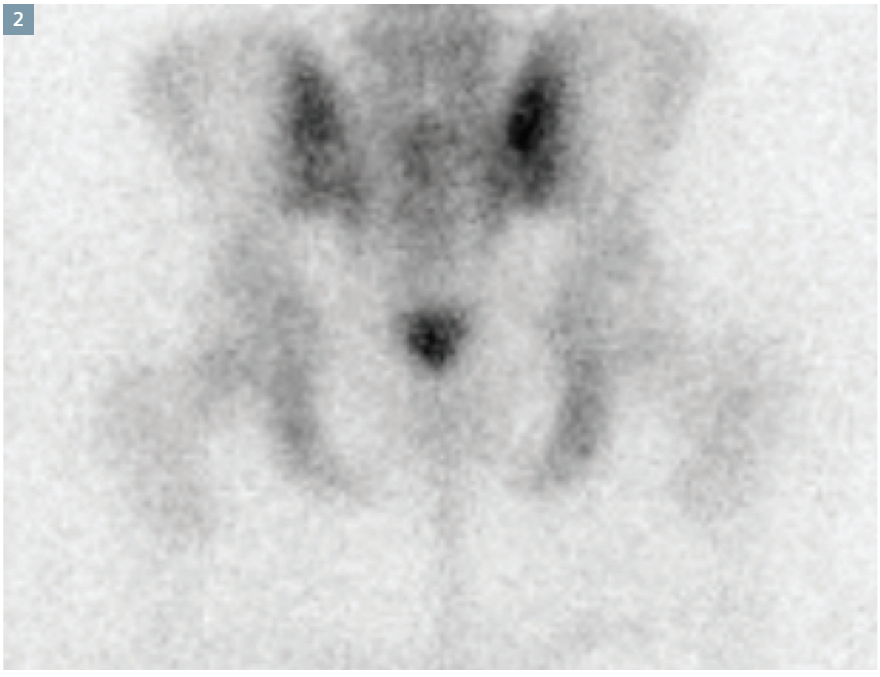

2 A planar spot view of posterior pelvis demonstrated increased uptake at the right sacroiliac joint area.

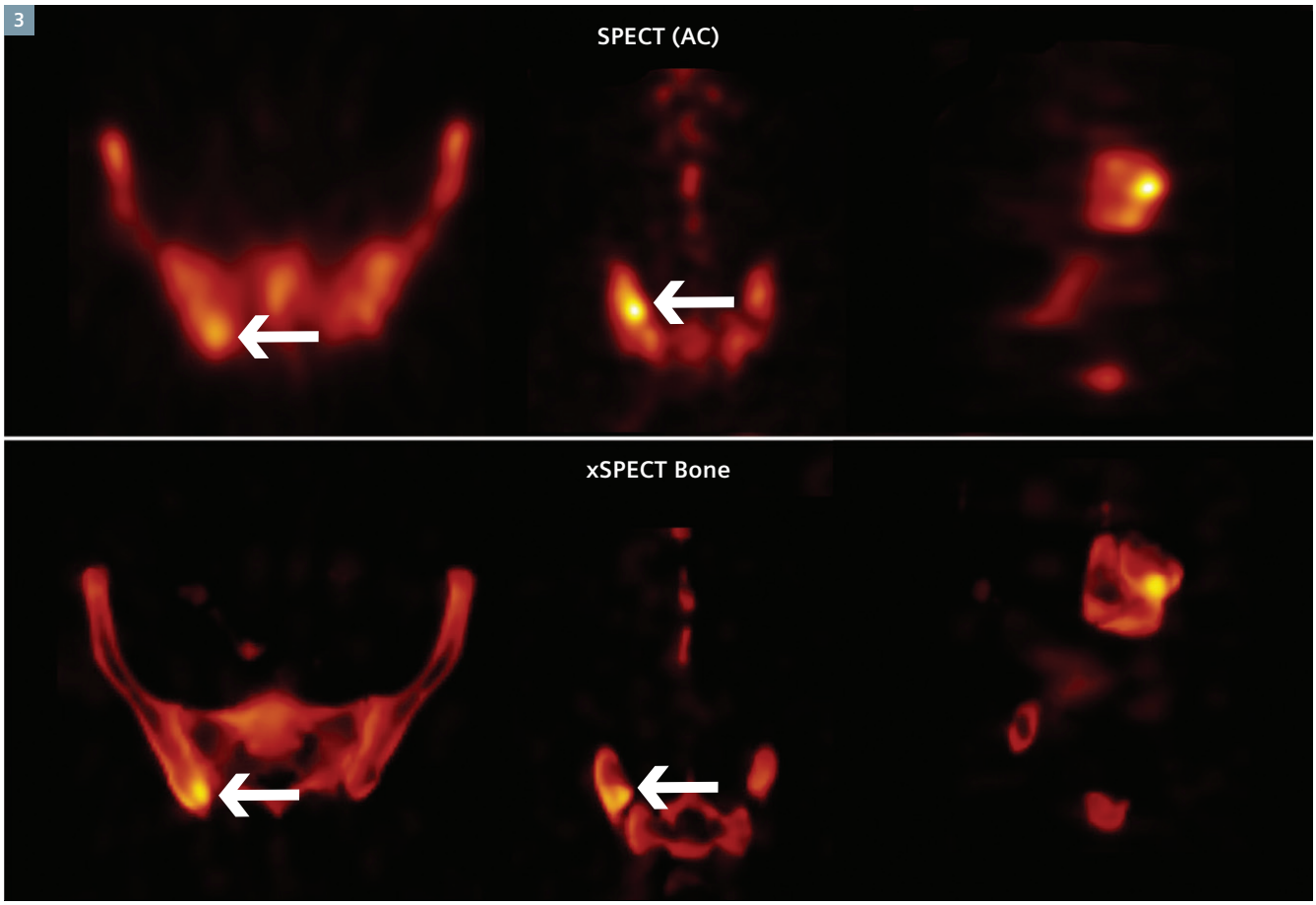

3 Comparison of SPECT (AC) and xSPECT reconstructed slices through the sacroiliac joint demonstrating a small hypermetabolic metastasis in the posterior right iliac bone.

Comments

The focal sclerotic and hypermetabolic skeletal lesion adjacent but distinctly separate from the sacroiliac joint demonstrated by xSPECT and CT is clearly suggestive of bone metastasis. Focally increased uptake is seen with both SPECT (AC) and xSPECT, but interpretation of xSPECT is facilitated by the sharper delineation of the iliac bone and the lesion itself.

Value of xSPECT Bone Technology

xSPECT Bone enables sharp delineation of focal skeletal metastases and the relationship with surrounding structures such as adjacent sacro-iliac joint and ala of the sacrum. Such clear delineation with xSPECT Bone helps ascertain potential complications secondary to possible expansion of the skeletal lesion, such as erosion of the outer cortical table, destruction of adjacent joint space and compression of nerve sheath.

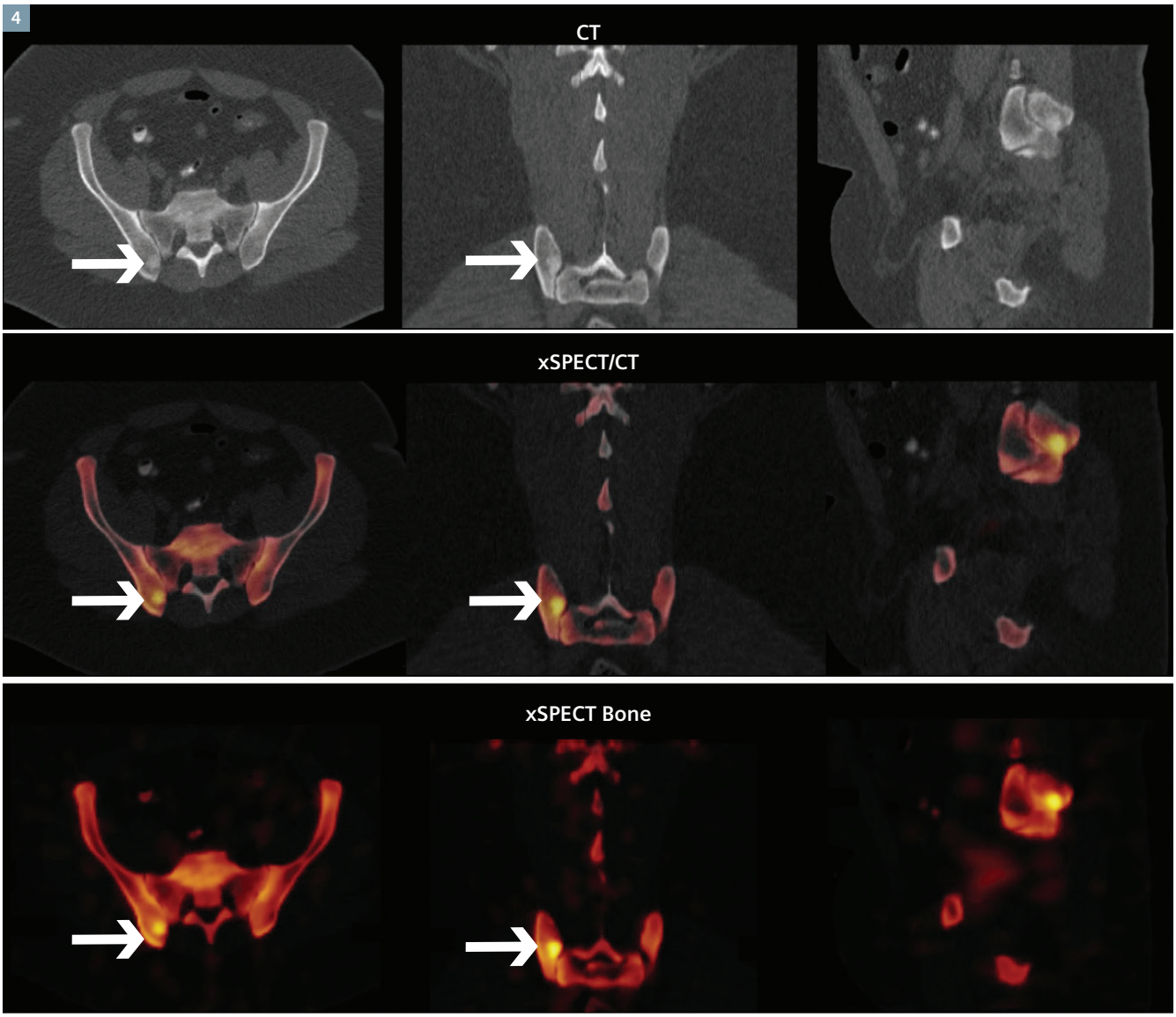

4 CT (*top row*) fusion of CT and xSPECT Bone (*middle row*) and xSPECT Bone (*bottom row*) demonstrates sclerotic focal bone lesion in the posterior aspect of the right ileum adjacent to the right sacroiliac joint suggestive of a skeletal metastasis.

Examination Protocol

Scanner	Symbia Intevo* with xSPECT
Scan dose	27 mCi ^{99m}Tc MDP
Scan delay	3 hours post injection
Parameters	64 frames 20 s/frame
Acquisition	Planar whole-body bone scan with spot views xSPECT study of the pelvis performed following planar study
CT	130 kV, 70 eff mAs 3mm slice thickness

* Symbia Intevo, xSPECT and xSPECT Bone are not commercially available in all countries. Due to regulatory reasons their future availability cannot be guaranteed. Please contact your local Siemens organization for further details.

The statements by Siemens' customers described herein are based on results that were achieved in the customer's unique setting. Since there is no "typical" hospital and many variables exist (e.g., hospital size, case mix, level of IT adoption) there can be no guarantee that other customers will achieve the same results.

Differentiation of Osteoarthritic Changes from Cortical Stress Fracture by xSPECT Bone

By: **Diego Davila, MD, Fellow Musculoskeletal Radiology & Nuclear Medicine, Johns Hopkins Medicine, MD, PhD, Professor, Dept of Radiology, Johns Hopkins Medicine, Baltimore, MD, USA**

Data courtesy of The Johns Hopkins Hospital, Baltimore, MD, USA

History

A 28-year-old man, who was a triathlete, presented with a chronic history of pain in the bilateral first metatarsophalangeal joint, which was more severe in the right foot. The patient was referred for a ^{99m}Tc methylene diphosphonate (MDP) bone scan. Planar and xSPECT* study was performed on a Symbia Intevo™* with xSPECT Bone*.

Diagnosis

xSPECT Bone shows focal increase in uptake within the first metatarsophalangeal joint exactly corresponding to the joint space and adjacent subchondral regions. Increased uptake corresponds to osteophytes on the dorsal subarticular margin of the distal end of the first metatarsal. CT shows subchondral sclerosis and joint space narrowing, which, in addition to the overhanging osteophytes, indicates severe degenerative joint disease. Despite mild sclerosis of the sesamoids, no abnormal tracer uptake is noted within them on either side. xSPECT Bone shows focal increase in uptake of ^{99m}Tc MDP in the right talocalcaneal joint space (Figure 5) exactly corresponding to a bulky osteophyte within the joint space, which suggests osteoarthritic changes. The sharp definition of the focal uptake limited to and exactly corresponding to the osteophyte within the joint space with clear delineation of absence of degenerative change in the rest of the joint margins reflects the high resolution and image quality achieved with xSPECT Bone.

A small focal area of slightly increased uptake of ^{99m}Tc MDP in the anterior and lateral articular facet of the lower right tibia is demonstrated on xSPECT Bone (*Figure 6*). The focal uptake exactly corresponds to a very small osteophyte. CT shows a sclerotic growth plate scar without cortical disruption, displacement or joint space alteration. xSPECT Bone shows the articular uptake corresponding exactly to the small osteophyte and clearly separate and distinct from the growth plate sclerosis.

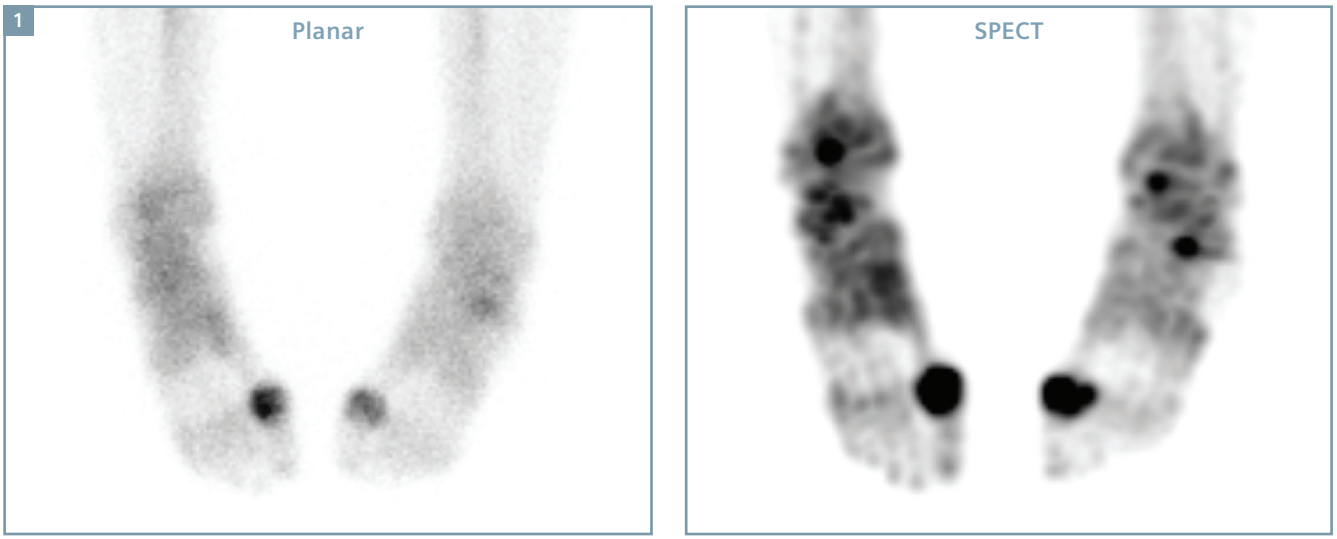

1 A planar spot view of the feet acquired in the delayed phase of a 3-phase bone scan shows increased uptake in both first metatarsophalangeal joints, the intensity being higher on the right foot. A SPECT MIP reconstruction of the feet shows enhanced uptake in the bilateral first metatarsophalangeal joints along with small focal hot areas in the lower end of tibia and calcaneum on both sides. These focal lesions are not well visualized on the planar study.

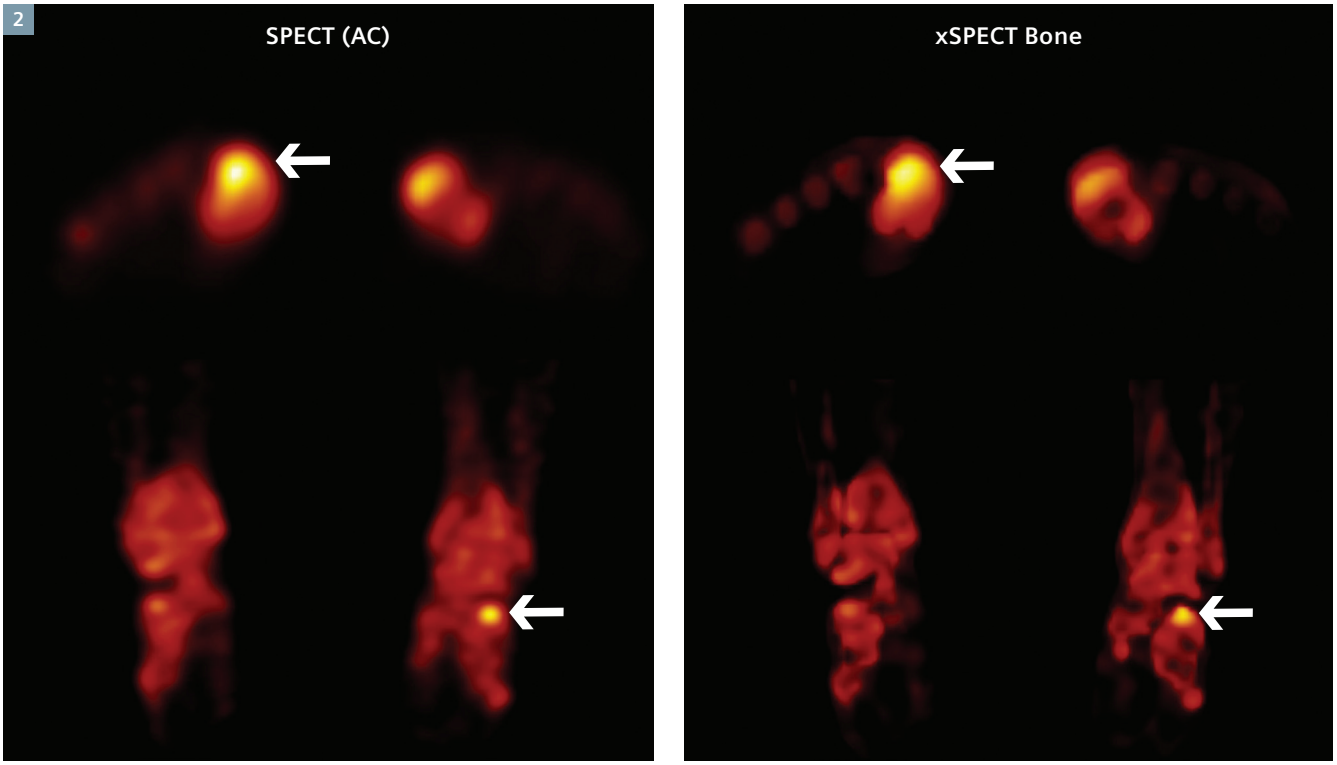

2 A comparison of xSPECT Bone and conventional SPECT (AC) shows sharper definition of ^{99m}Tc MDP uptake in the articular surface of distal end of the bilateral first metatarsal, as well as a small focal hot lesion in the left talo-calcaneal joint space.

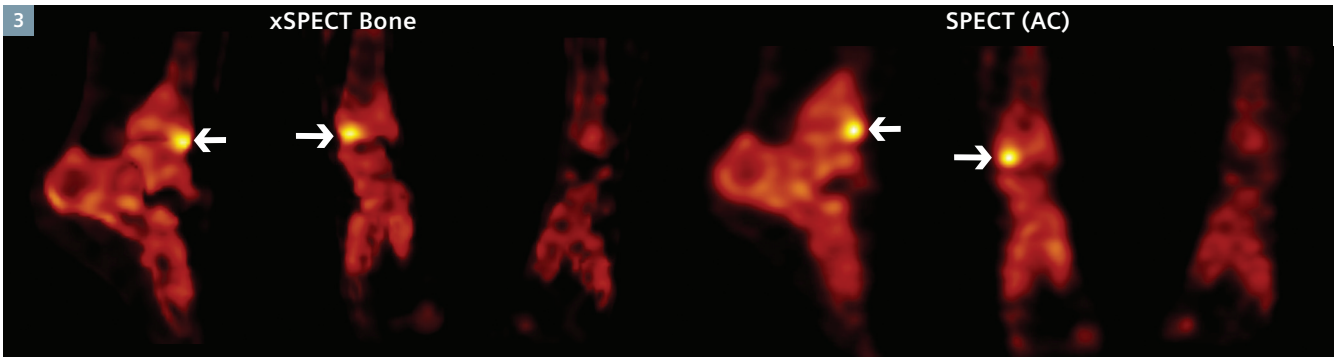

3 A comparison of xSPECT Bone and SPECT (AC) shows sharp delineation of focal uptake at the articular surface of lower end of right tibia.

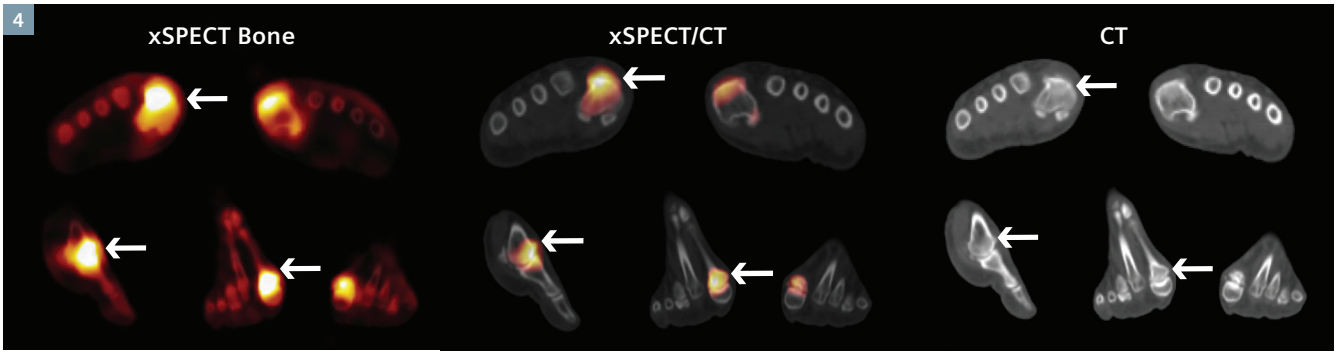

4 xSPECT Bone, fused xSPECT Bone + CT and CT images show severe degenerative changes in the first metatarsophalangeal joint.

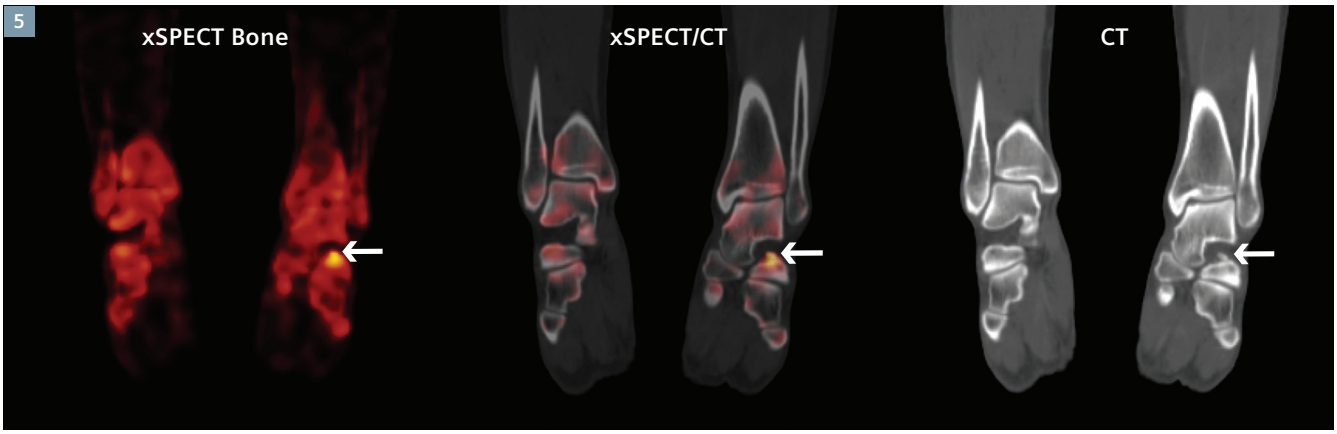

5 xSPECT Bone, CT and fused images of CT and xSPECT Bone show hypermetabolic osteophyte in the talo-calcaneal joint space suggestive of osteoarthritis.

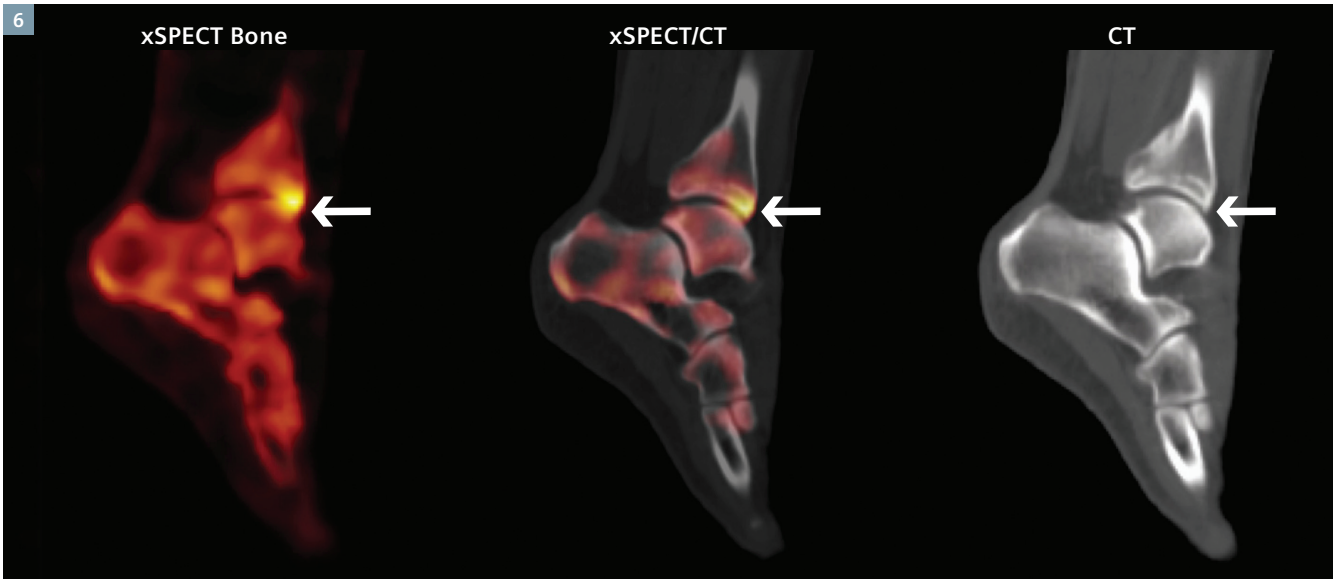

6 xSPECT Bone and CT shows focal increase in uptake at the anterior edge of the tibial articular surface corresponding to a small osteophyte. The xSPECT Bone and CT fusion image shows the uptake to correspond exactly to the anterolateral edge of the articular surface without involving the cortical sclerotic growth plate scar.

Comments

Absence of significant uptake at the tibial cortical growth plate sclerosis and exact coregistration of tibial articular surface uptake to a very small osteophyte suggests that the articular uptake is related to osteoarthritic changes rather than stress cortical injury. xSPECT Bone could help physicians identify early osteoarthritic changes related to small osteophyte and exclude cortical stress injury, which is also common in long distance runners. Ongoing growth of the tibial articular spur may lead to anterior impingement. Definition of osteophyte reflecting osteoarthritic changes and differentiation from stress injury by xSPECT may direct more proactive management to prevent subsequent development of anterior impingement.

Value of xSPECT Bone Technology

xSPECT Bone sharply delineates uptake in the talo-calcaneal joint space, which exactly corresponds to the osteophyte on the CT. Such sharp delineation improves the diagnostic confidence to exclude other conditions, such as a stress fracture, and helps plan subsequent management.

Examination Protocol

Scanner	Symbia Intevo with xSPECT Bone
Scan dose	25 mCi (925 MBq) ^{99m}Tc MDP
Scan delay	3 hours post injection
Parameters	64 frames, 25 sec/frame
CT	130 kV, 60 eff mAs, 3mm slice thickness

* Symbia Intevo, xSPECT and xSPECT Bone are not commercially available in all countries. Due to regulatory reasons their future availability cannot be guaranteed. Please contact your local Siemens organization for further details.

The statements by Siemens customers described herein are based on results that were achieved in the customer's unique setting. Since there is no "typical" hospital and many variable exist (e.g., hospital size, case mix, level of IT adoption) there can be no guarantee that other customers will achieve the same results.

Quantitative SPECT Imaging of Hepato-Pulmonary Shunting Prior to SIR-Spheres Treatment

By: **Kathy P. Willowson, PhD, and Dale L. Bailey, PhD, Department of Nuclear Medicine, Royal North Shore Hospital and Institute of Medical Physics, University of Sydney, Sydney, Australia**

Data courtesy of Royal North Shore Hospital, Sydney, Australia

Case 1: History

A 27-year-old male, suffering from extensive liver metastases from colorectal cancer, was referred for radionuclide therapy. A liver/lung shunt study was performed with [^{99m}Tc]-macro-aggregated-albumin (MAA) to evaluate the patient's suitability for SIR-Spheres therapy (Sirtex Medical, Sydney, AUS).

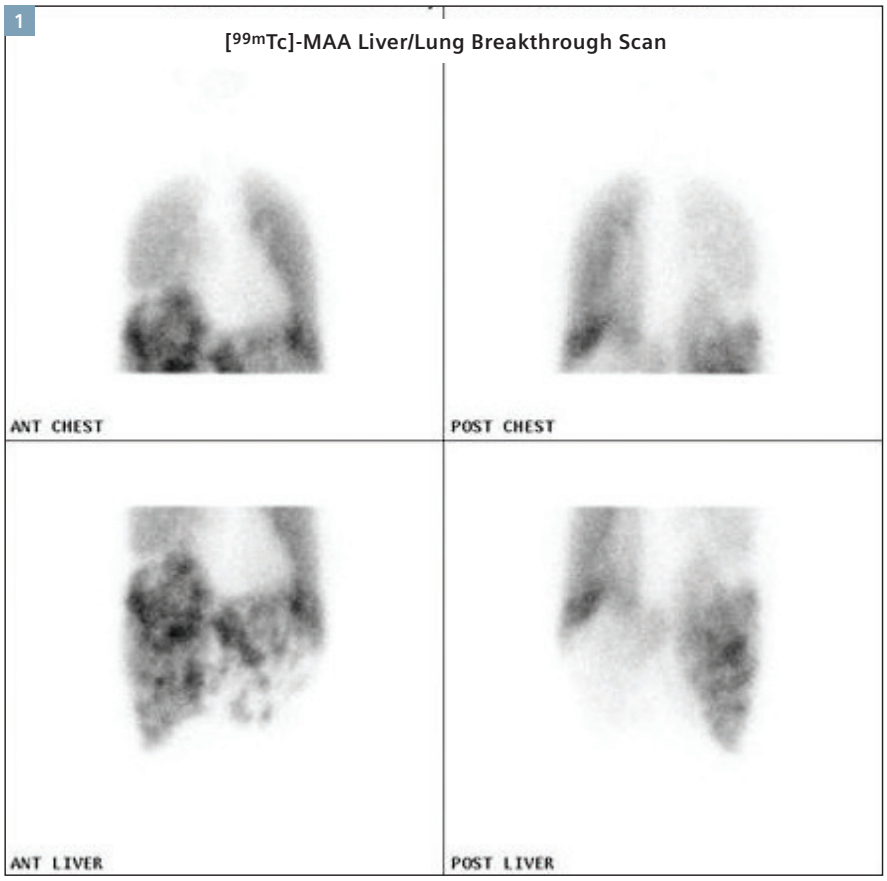

1 Planar (*Figure 1*) and SPECT•CT (*Figure 2, pg. 45*) images for lung shunt derivation following [^{99m}Tc]-MAA shunt study in evaluation for SIR-Spheres therapy demonstrates extensive arterio-venous (A-V) shunting to the lungs.

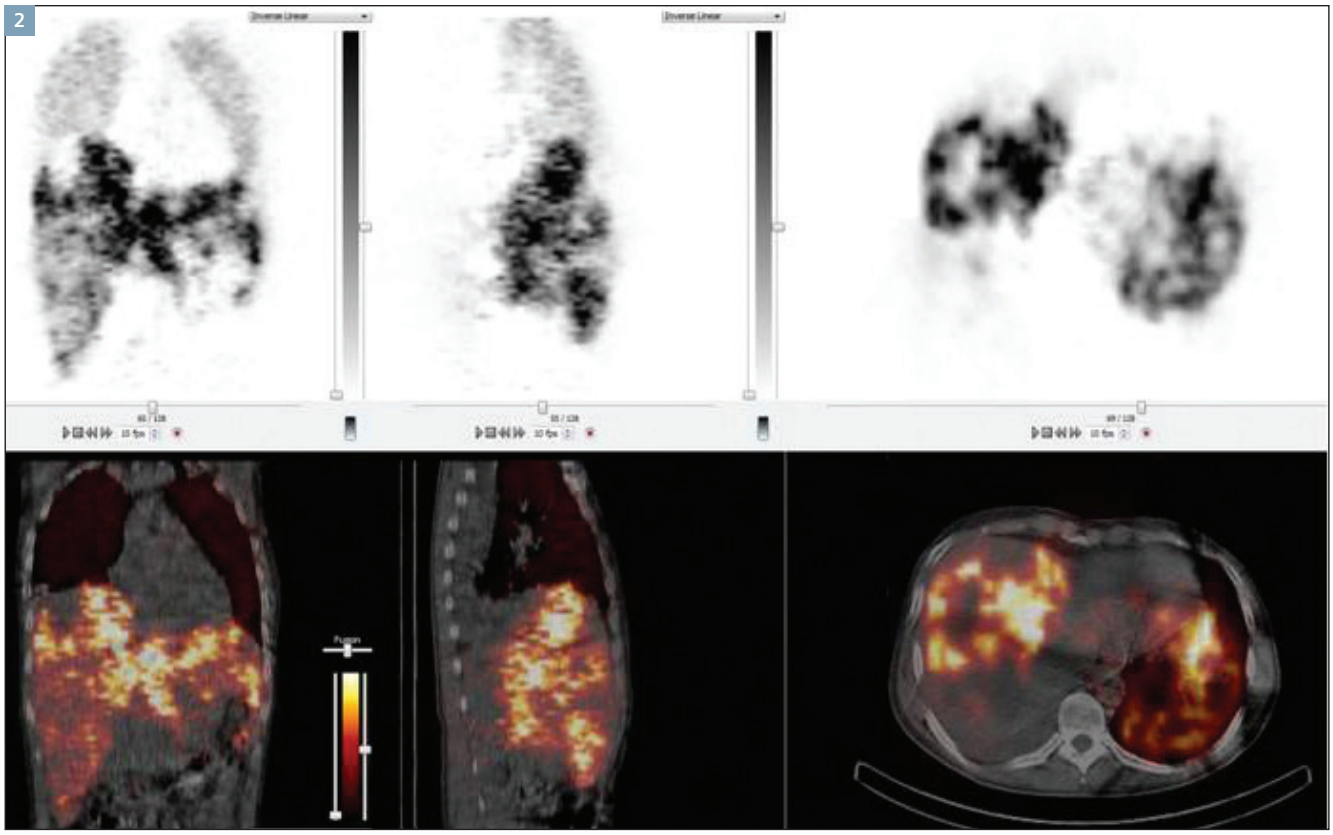

2 Planar (*Figure 1, pg. 44*) and SPECT•CT (*Figure 2*) images for lung shunt derivation following [^{99m}Tc]-MAA shunt study in evaluation for SIR-Spheres therapy demonstrates extensive arteriovenous (A-V) shunting to the lungs.

Diagnosis

Standard analysis by planar whole-body imaging, and hand-drawn regions of interest (ROIs) over the liver and lungs, yielded a shunt fraction of 57%, greatly exceeding the accepted limit for treatment (≤20%). Fully quantitative SPECT•CT, with CT-derived ROIs around the lung and liver, was used for a more accurate assessment of shunting. The total amount of radioactivity in the lungs was measured to be 21 MBq of the 137 MBq that was administered (15%).

An independent measure of lung radioactivity, using a second injection of a calibrated amount of [^{99m}Tc]-MAA given intravenously, estimated this fraction to be 23 ±5%. The quantitative SPECT measured 70 MBq for total deposition in liver, resulting in a lung-to-liver shunt fraction of 30%. The lung and liver radioactivity accounted for approximately 66% of the total radioactivity administered, and 88% of what was measured in the SPECT field-of-view. Other sites of accumulation of the radiotracer were noted (e.g., thyroid) on the whole-body planar images.

Comments

The patient demonstrated A-V shunting far greater than acceptable, and so did not proceed to therapy. Quantitative SPECT•CT was useful in deriving a more accurate shunting measurement. The measured fraction of injected dose present in the lungs could be used to estimate absorbed dose-to-lungs at therapy. In this case, assuming a 2 GBq SIR-Spheres dose, quantitative SPECT indicates that 15 Gy would be delivered to the lung tissue at therapy. While acceptable (below 25 Gy), it relies on the assumption that the lung activity is evenly distributed, and that the A-V shunting seen on the MAA work-up study will be replicated at therapy. Due to uncertainties associated with these assumptions, the Sirtex guidelines should be followed when evaluating patients for therapy.

Value of Technology

SPECT•CT has significantly improved exact localization of extra-hepatic shunt of [^{99m}Tc]-MAA in patients with liver tumors being evaluated for ^{90}Y microsphere radio embolization therapy. Correct localization and quantification of extra-hepatic shunting is key to further management decision-making for SIRT—which is made possible with SPECT and diagnostic CT combinations.

Case 2: History

A 63-year-old male, with metastatic melanoma in the liver, received 1.9 GBq [^{90}Y]-SIR-Spheres for treatment of liver-borne disease. The pre-therapy, planar imaging work-up demonstrated an acceptable shunt of 2.6%. Pre-therapy [^{99m}Tc]-MAA-SPECT•CT was performed on a Symbia™ T6. Twenty-four hours following the infusion of therapeutic dose of [^{90}Y]-SIR-Spheres, a PET/CT study with contrast CT was performed on a Biograph™ mCT.

Diagnosis

Quantitative analysis of the [^{99m}Tc]-MAA-SPECT•CT study showed that 72% of the injected activity was localized to the liver (some free pertechnetate was seen outside the field of view of the SPECT), with 15% of the total amount administered localizing in the tumor (as defined on CT). There was good correlation between the [^{99m}Tc]-MAA-SPECT and the localization of [^{90}Y]-SIR-Spheres (PET) post-implantation. The lesions seen on the contrast-enhanced CT were well targeted by the treatment. The quantitative [^{99m}Tc]-MAA-SPECT•CT study was used to generate dose volume histograms (DVHs) of the tumor and healthy liver, assuming 100% (minus lung-shunt value) of the prescribed ^{90}Y would be trapped in the liver. Predicted absorbed dose estimates were made for the time of therapy, which were compared with actual DVHs from the [^{90}Y]-PET. The liver and tumor were predicted to receive a mean dose of 30.6 Gy and 92.7 Gy, respectively. The post-treatment analysis estimated an actual delivered mean-dose of 30.8 Gy and 85.9 Gy, with 72% of the tumor receiving greater than 50 Gy.

Quantitative SPECT allowed estimates of absorbed dose to volumes of interest to be predicted prior to treatment. In this case, the estimates compared favorably to the actual results from post-implantation imaging. Use of a reliable and accurate surrogate for shunt assessment, combined with quantitative SPECT, can potentially allow dose estimates to be used for improved treatment planning.

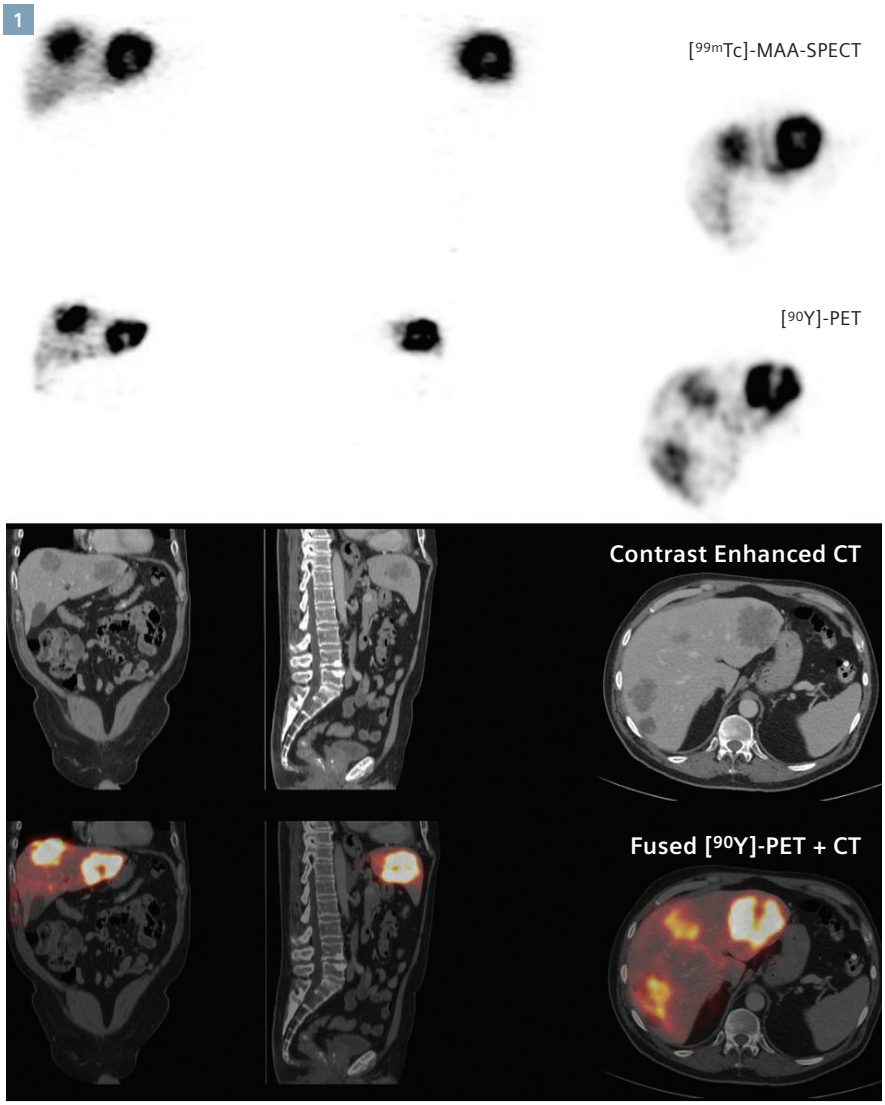

1 Imaging for the patient undergoing SIR-Spheres treatment for liver metastases from melanoma. Good correlation is seen between the [^{99m}Tc]-MAA-SPECT (from pre-treatment shunt study) and [^{90}Y]-SIR-Spheres, as imaged by PET•CT 24 hours post-implantation. Treatment localized well to areas of disease demonstrated on the contrast-enhanced CT, with the large lesion of the left lobe exhibiting uptake around the rim and absence in the necrotic center.

Comments

The shunt fraction computed, using standard methods on planar images of the liver and lungs, is semiempirical, as it does not normally include any correction for photon attenuation, which is different for the liver and lungs due to air in the thorax. Hence, while reduction in the administered amount of the therapeutic radioactivity can be implemented, depending on the fraction, it does not give a true indication of the amount of radiation bypassing the liver and depositing in the lung. This was seen in Case 1 when the amount of lung shunting,

2

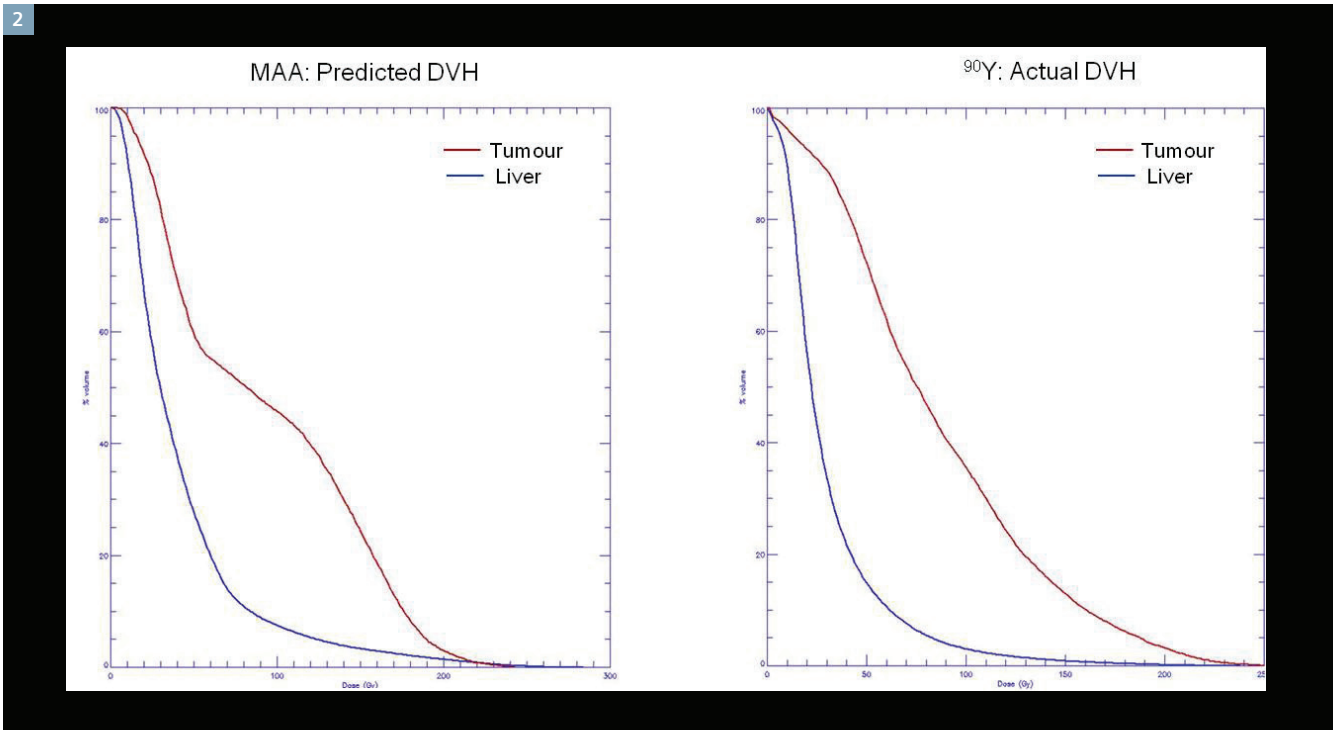

2 Dose volume histograms comparing the predicted dose distribution in tumor and liver from quantitative SPECT ([^{99m}Tc]-MAA shunt study) and quantitative PET (^{90}Y post-implantation).

calculated by comparing the liver and lung ROIs on 2D whole-body planar imaging, appears to have greatly overestimated the actual fraction bypassing the liver and depositing in the lungs. Quantitative SPECT can provide this, permitting a direct comparison between SPECT and PET as in Case 2. The quantitative information obtained can be used to convert the measured radioactivity burden into an estimated radiation dose (MIRD methodology) and derive DVHs for the liver. This will give a better indication of the suitability of SIRT treatment and the maximum tolerable dose that can be delivered to effect tumor control while restricting liver and lung doses to tolerable levels. It will also enhance our understanding of the dose-response relationship for this type of therapy.

Value of Technology

Quantification with SPECT•CT is made possible with CT attenuation correction and isotope-specific calibrations. Such quantitative measurements enable absorbed dose calculations for ^{90}Y radio embolization based on [^{99m}Tc]-MAA uptake in the tumor and non-target liver and lung.

Examination Protocol

Scanner	Symbia T6
Scan dose	Case 1: 137 MBq (3.7 mCi) [^{99m}Tc]-MAA Case 2: 150 MBq (4.1 mCi) [^{99m}Tc]-MAA
Scan protocol	120 frames (60 per detector) 20 s/frame

The statements by Siemens customers described herein are based on results that were achieved in the customer's unique setting. Since there is no "typical" hospital and many variable exist (e.g., hospital size, case mix, level of IT adoption) there can be no guarantee that other customers will achieve the same results.

References:
1 **Bailey DL, Willowson KP.** An Evidence-Based Review of Quantitative SPECT Imaging and Potential Clinical Applications. *J Nucl Med*. 2013;54(1):83–9.
2 **Willowson K, Bailey DL, Baldock C.** Quantifying lung shunting during planning for radio-embolization. *Phys Med Biol*. 2011 Jul 7;56(13):N145-52.

Publisher:
Siemens Medical Solutions USA, Inc.
Healthcare Sector Molecular Imaging
2501 N. Barrington Road
Hoffman Estates, IL 60192
USA
Telephone: + 1 847 304-7700
www.siemens.com/mi

Editor: Terri McGuire
therese.mcguire@siemens.com

Editor: Rhett Morici
rhett.morici@siemens.com

Responsible for Content:
Partha Ghosh
partha.ghosh@siemens.com

Design Consulting:
VieceliDesign, Inc., Utah, USA

Printer: Tewell Warren Printing,
Colorado, USA

Note in accordance with § 33 Para.1 of the German Federal Data Protection Law: Dispatch is made using an address file which is maintained with the aid of an automated data processing system.

We remind our readers that when printed, X-ray films never disclose all the information content of the original. Artifacts in CT, MR, SPECT, SPECT/CT, PET, PET/CT and PET/MR images are recognizable by their typical features and are generally distinguishable from existing pathology. As referenced below, healthcare practioners are expected to utilize their own learning, training and expertise in evaluating images.

Please contact your local Siemens sales representative for the most current information.

Note: Original images always lose a certain amount of detail when reproduced. All comparative claims derived from competitive data at the time of printing. Data on file.

The consent of the authors and publisher are required for the reprint or reuse of an article. Please contact Siemens for further information. Suggestions, proposals and information are always welcome; they are carefully examined and submitted to the editorial board for attention. Imaging Life is not responsible for loss, damage or any other injury to unsolicited manuscripts or materials.

We welcome your questions and comments about the editorial content of Imaging Life. Please contact us at imaginglife.healthcare@siemens.com.

Imaging Life is available on the internet: www.siemens.com/imaginglife

Imaging Life also has a free iPad and iPhone App available. From your iPad or iPhone, go to the App Store and search "Imaging Life," then download.

Some of the imaging biomarkers in this publication are not currently recognized by the U.S. Food and Drug Administration (FDA) or other regulatory agencies as being safe and effective, and Siemens does not make any claims regarding their use.

Clinical Images Courtesy of:

Pg. 4-7 University of Michigan, Ann Arbor, MI, USA;
Pg. 8-15 University of Tennessee, Knoxville, TN, USA;
Pg. 16-19 Parkway Hospitals, Singapore;
Pg. 20-23 Xinhua Hospital, Shanghai, China;
Pg. 24-27 Department of Nuclear Medicine, Katharinenhospital Klinikum, Stuttgart, Germany;
Pg. 28-31 Eberhard Karis University, Tübingen, Germany;
Pg. 32-43 The Johns Hopkins Hospital, Baltimore, MD, USA;
Pg. 44-47 Royal North Shore Hospital, Sydney, Australia

DISCLAIMERS: Imaging Life: "The information presented in this magazine is for illustration only and is not intended to be relied upon by the reader for instruction as to the practice of medicine. Healthcare practitioners reading this information are reminded that they must use their own learning, training and expertise in dealing with their individual patients. This material does not substitute for that duty and is not intended by Siemens Healthcare to be used for any purpose in that regard." Contrast Agents: "The drugs and doses mentioned herein are consistent with the approved labeling for uses and/or indications of the drug. The treating physician bears the sole responsibility for the diagnosis and treatment of patients, including drugs and doses prescribed in connection with such use. The Operating Instructions must always be strictly followed when operating your Siemens system. The source for the technical data is the corresponding data sheets." Trademarks: "All trademarks mentioned in this document are property of their respective owners." Results: "The outcomes achieved by the Siemens customers described herein were achieved in the customer's unique setting. Since there is no "typical" hospital and many variables exist (e.g., hospital size, case mix, level of IT adoption), there can be no guarantee that others will achieve the same results."

HIGHLIGHTS OF PRESCRIBING INFORMATION

These highlights do not include all the information needed to use Fludeoxyglucose F 18 Injection safely and effectively. See full prescribing information for Fludeoxyglucose F 18 Injection.

Fludeoxyglucose F 18 Injection, USP

For intravenous use

Initial U.S. Approval: 2005

RECENT MAJOR CHANGES

Warnings and Precautions (5.1, 5.2) 7/2010

Adverse Reactions (6) 7/2010

INDICATIONS AND USAGE

Fludeoxyglucose F18 Injection is indicated for positron emission tomography (PET) imaging in the following settings:

- Oncology: For assessment of abnormal glucose metabolism to assist in the evaluation of malignancy in patients with known or suspected abnormalities found by other testing modalities, or in patients with an existing diagnosis of cancer.
- Cardiology: For the identification of left ventricular myocardium with residual glucose metabolism and reversible loss of systolic function in patients with coronary artery disease and left ventricular dysfunction, when used together with myocardial perfusion imaging.
- Neurology: For the identification of regions of abnormal glucose metabolism associated with foci of epileptic seizures (1).

DOSAGE AND ADMINISTRATION

Fludeoxyglucose F 18 Injection emits radiation. Use procedures to minimize radiation exposure. Screen for blood glucose abnormalities.

- In the oncology and neurology settings, instruct patients to fast for 4 to 6 hours prior to the drug's injection. Consider medical therapy and laboratory testing to assure at least two days of normoglycemia prior to the drug's administration (5.2).
- In the cardiology setting, administration of glucose-containing food or liquids (e.g., 50 to 75 grams) prior to the drug's injection facilitates localization of cardiac ischemia (2.3).

Aseptically withdraw Fludeoxyglucose F 18 Injection from its container and administer by intravenous injection (2).

The recommended dose:

- for adults is 5 to 10 mCi (185 to 370 MBq), in all indicated clinical settings (2.1).
- for pediatric patients is 2.6 mCi in the neurology setting (2.2).

Initiate imaging within 40 minutes following drug injection; acquire static emission images 30 to 100 minutes from time of injection (2).

DOSAGE FORMS AND STRENGTHS

Multi-dose 30mL and 50mL glass vial containing 0.74 to 7.40 GBq/mL (20 to 200 mCi/mL) Fludeoxyglucose F 18 Injection and 4.5mg of sodium chloride with 0.1 to 0.5% w/w ethanol as a stabilizer (approximately 15 to 50 mL volume) for intravenous administration (3).

CONTRAINDICATIONS

None

WARNINGS AND PRECAUTIONS

- Radiation risks: use smallest dose necessary for imaging (5.1).
- Blood glucose adnormalities: may cause suboptimal imaging (5.2).

ADVERSE REACTIONS

Hypersensitivity reactions have occurred; have emergency resuscitation equipment and personnel immediately available (6).

To report SUSPECTED ADVERSE REACTIONS, contact PETNET Solutions, Inc. at 877-473-8638 or FDA at 1-800-FDA-1088 or www.fda.gov/medwatch.

USE IN SPECIFIC POPULATIONS

Pregnancy Category C: No human or animal data. Consider alternative diagnostics; use only if clearly needed (8.1).

- Nursing mothers: Use alternatives to breast feeding (e.g., stored breast milk or infant formula) for at least 10 half-lives of radioactive decay, if Fludeoxyglucose F 18 Injection is administered to a woman who is breast-feeding (8.3).
- Pediatric Use: Safety and effectiveness in pediatric patients have not been established in the oncology and cardiology settings (8.4).

See 17 for PATIENT COUNSELING INFORMATION

Revised: 1/2011

FULL PRESCRIBING INFORMATION: CONTENTS*

* Sections or subsections omitted from the full prescribing information are not listed.

FULL PRESCRIBING INFORMATION

1 INDICATIONS AND USAGE

Fludeoxyglucose F 18 Injection is indicated for positron emission tomography (PET) imaging in the following settings:

1.1 Oncology

For assessment of abnormal glucose metabolism to assist in the evaluation of malignancy in patients with known or suspected abnormalities found by other testing modalities, or in patients with an existing diagnosis of cancer.

1.2 Cardiology

For the identification of left ventricular myocardium with residual glucose metabolism and reversible loss of systolic function in patients with coronary artery disease and left ventricular dysfunction, when used together with myocardial perfusion imaging.

1.3 Neurology

For the identification of regions of abnormal glucose metabolism associated with foci of epileptic seizures.

2 DOSAGE AND ADMINISTRATION

Fludeoxyglucose F 18 Injection emits radiation. Use procedures to minimize radiation exposure. Calculate the final dose from the end of synthesis (EOS) time using proper radioactive decay factors. Assay the final dose in a properly calibrated dose calibrator before administration to the patient [see Description (11.2)].

2.1 Recommended Dose for Adults

Within the oncology, cardiology and neurology settings, the recommended dose for adults is 5 to 10 mCi (185 to 370 MBq) as an intravenous injection.

2.2 Recommended Dose for Pediatric Patients

Within the neurology setting, the recommended dose for pediatric patients is 2.6 mCi, as an intravenous injection. The optimal dose adjustment on the basis of body size or weight has not been determined [see Use in Special Populations (8.4)].

2.3 Patient Preparation

- To minimize the radiation absorbed dose to the bladder, encourage adequate hydration. Encourage the patient to drink water or other fluids (as tolerated) in the 4 hours before their PET study.
- Encourage the patient to void as soon as the imaging study is completed and as often as possible thereafter for at least one hour.
- Screen patients for clinically significant blood glucose abnormalities by obtaining a history and/or laboratory tests [see Warnings and Precautions (5.2)]. Prior to Fludeoxyglucose F 18 PET imaging in the oncology and neurology settings, instruct patient to fast for 4 to 6 hours prior to the drug's injection.
- In the cardiology setting, administration of glucose-containing food or liquids (e.g., 50 to 75 grams) prior to Fludeoxyglucose F18 Injection facilitates localization of cardiac ischemia

2.4 Radiation Dosimetry

The estimated human absorbed radiation doses (rem/mCi) to a newborn (3.4 kg), 1-year old (9.8 kg), 5-year old (19 kg), 10-year old (32 kg), 15-year old (57 kg), and adult (70 kg) from intravenous administration of Fludeoxyglucose F 18 Injection are shown in Table 1. These estimates were calculated based on human[2] data and using the data published by the International Commission on Radiological Protection[4] for Fludeoxyglucose ^{18}F. The dosimetry data show that there are slight variations in absorbed radiation dose for various organs in each of the age groups. These dissimilarities in absorbed radiation dose are due to developmental age variations (e.g., organ size, location, and overall metabolic rate for each age group). The identified critical organs (in descending order) across all age groups evaluated are the urinary bladder, heart, pancreas, spleen, and lungs.

Table 1. Estimated Absorbed Radiation Doses (rem/mCi) After Intravenous Administration of Fludeoxyglucose F-18 Injection[a]

Organ	Newborn (3.4 kg)	1-year old (9.8 kg)	5-year old (19 kg)	10-year old (32 kg)	15-year old (57 kg)	Adult (70 kg)
Bladder wall[b]	4.3	1.7	0.93	0.60	0.40	0.32
Heart wall	2.4	1.2	0.70	0.44	0.29	0.22
Pancreas	2.2	0.68	0.33	0.25	0.13	0.096
Spleen	2.2	0.84	0.46	0.29	0.19	0.14
Lungs	0.96	0.38	0.20	0.13	0.092	0.064
Kidneys	0.81	0.34	0.19	0.13	0.089	0.074
Ovaries	0.80	0.8	0.19	0.11	0.058	0.053
Uterus	0.79	0.35	0.19	0.12	0.076	0.062
LLI wall *	0.69	0.28	0.15	0.097	0.060	0.051
Liver	0.69	0.31	0.17	0.11	0.076	0.058
Gallbladder wall	0.69	0.26	0.14	0.093	0.059	0.049
Small intestine	0.68	0.29	0.15	0.096	0.060	0.047
ULI wall **	0.67	0.27	0.15	0.090	0.057	0.046
Stomach wall	0.65	0.27	0.14	0.089	0.057	0.047
Adrenals	0.65	0.28	0.15	0.095	0.061	0.048
Testes	0.64	0.27	0.14	0.085	0.052	0.041
Red marrow	0.62	0.26	0.14	0.089	0.057	0.047
Thymus	0.61	0.26	0.14	0.086	0.056	0.044
Thyroid	0.61	0.26	0.13	0.080	0.049	0.039
Muscle	0.58	0.25	0.13	0.078	0.049	0.039
Bone surface	0.57	0.24	0.12	0.079	0.052	0.041
Breast	0.54	0.22	0.11	0.068	0.043	0.034
Skin	0.49	0.20	0.10	0.060	0.037	0.030
Brain	0.29	0.13	0.09	0.078	0.072	0.070
Other tissues	0.59	0.25	0.13	0.083	0.052	0.042

[a] MIRDOSE 2 software was used to calculate the radiation absorbed dose. Assumptions on the biodistribution based on data from Gallagher et al.1 and Jones et al.2

[b] The dynamic bladder model with a uniform voiding frequency of 1.5 hours was used. *LLI = lower large intestine; **ULI = upper large intestine

2.5 Radiation Safety – Drug Handling

- Use waterproof gloves, effective radiation shielding, and appropriate safety measures when handling Fludeoxyglucose F 18 Injection to avoid unnecessary radiation exposure to the patient, occupational workers, clinical personnel and other persons.
- Radiopharmaceuticals should be used by or under the control of physicians who are qualified by specific training and experience in the safe use and handling of radionuclides, and whose experience and training have been approved by the appropriate governmental agency authorized to license the use of radionuclides.
- Calculate the final dose from the end of synthesis (EOS) time using proper radioactive decay factors. Assay the final dose in a properly calibrated dose calibrator before administration to the patient [see Description (11.2)].
- The dose of Fludeoxyglucose F 18 used in a given patient should be minimized consistent with the objectives of the procedure, and the nature of the radiation detection devices employed.

2.6 Drug Preparation and Administration

- Calculate the necessary volume to administer based on calibration time and dose.
- Aseptically withdraw Fludeoxyglucose F 18 Injection from its container.
- Inspect Fludeoxyglucose F 18 Injection visually for particulate matter and discoloration before administration, whenever solution and container permit.
- Do not administer the drug if it contains particulate matter or discoloration; dispose of these unacceptable or unused preparations in a safe manner, in compliance with applicable regulations.
- Use Fludeoxyglucose F 18 Injection within 12 hours from the EOS.

2.7 Imaging Guidelines

- Initiate imaging within 40 minutes following Fludeoxyglucose F 18 Injection administration.
- Acquire static emission images 30 to 100 minutes from the time of injection.

3 DOSAGE FORMS AND STRENGTHS

Multiple-dose 30 mL and 50 mL glass vial containing 0.74 to 7.40 GBq/mL (20 to 200 mCi/mL) of Fludeoxyglucose F 18 Injection and 4.5 mg of sodium chloride with 0.1 to 0.5% w/w ethanol as a stabilizer (approximately 15 to 50 mL volume) for intravenous administration.

4 CONTRAINDICATIONS

None

5 WARNINGS AND PRECAUTIONS

5.1 Radiation Risks

Radiation-emitting products, including Fludeoxyglucose F 18 Injection, may increase the risk for cancer, especially in pediatric patients. Use the smallest dose necessary for imaging and ensure safe handling to protect the patient and health care worker [see Dosage and Administration (2.5)].

5.2 Blood Glucose Abnormalities

In the oncology and neurology setting, suboptimal imaging may occur in patients with inadequately regulated blood glucose levels. In these patients, consider medical therapy and laboratory testing to assure at least two days of normoglycemia prior to Fludeoxyglucose F 18 Injection administration.

6 ADVERSE REACTIONS

Hypersensitivity reactions with pruritus, edema and rash have been reported in the postmarketing setting. Have emergency resuscitation equipment and personnel immediately available.

7 DRUG INTERACTIONS

The possibility of interactions of Fludeoxyglucose F 18 Injection with other drugs taken by patients undergoing PET imaging has not been studied.

8 USE IN SPECIFIC POPULATIONS

8.1 Pregnancy

Pregnancy Category C

Animal reproduction studies have not been conducted with Fludeoxyglucose F 18 Injection. It is also not known whether Fludeoxyglucose F 18 Injection can cause fetal harm when administered to a pregnant woman or can affect reproduction capacity. Consider alternative diagnostic tests in a pregnant woman; administer Fludeoxyglucose F 18 Injection only if clearly needed.

8.3 Nursing Mothers

It is not known whether Fludeoxyglucose F 18 Injection is excreted in human milk. Consider alternative diagnostic tests in women who are breast-feeding. Use alternatives to breast feeding (e.g., stored breast milk or infant formula) for at least 10 half-lives of radioactive decay, if Fludeoxyglucose F 18 Injection is administered to a woman who is breast-feeding.

8.4 Pediatric Use

The safety and effectiveness of Fludeoxyglucose F 18 Injection in pediatric patients with epilepsy is established on the basis of studies in adult and pediatric patients. In pediatric patients with epilepsy, the recommended dose is 2.6 mCi. The optimal dose adjustment on the basis of body size or weight has not been determined. In the oncology or cardiology settings, the safety and effectiveness of Fludeoxyglucose F 18 Injection have not been established in pediatric patients.

11 DESCRIPTION

11.1 Chemical Characteristics

Fludeoxyglucose F 18 Injection is a positron emitting radiopharmaceutical that is used for diagnostic purposes in conjunction with positron emission tomography (PET) imaging. The active ingredient 2-deoxy-2-[^{18}F]fluoro-D-glucose has the molecular formula of $C_6H_{11}{}^{18}FO_5$ with a molecular weight of 181.26, and has the following chemical structure:

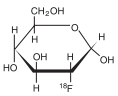

Fludeoxyglucose F 18 Injection is provided as a ready to use sterile, pyrogen free, clear, colorless solution. Each mL contains between 0.740 to 7.40GBq (20.0 to 200 mCi) of 2-deoxy-2-[^{18}F]fluoro-D-glucose at the EOS, 4.5 mg of sodium chloride and 0.1 to 0.5% w/w ethanol as a stabilizer. The pH of the solution is between 4.5 and 7.5. The solution is packaged in a multiple-dose glass vial and does not contain any preservative.

11.2 Physical Characteristics

Fluorine F 18 decays by emitting positron to Oxygen O 16 (stable) and has a physical half-life of 109.7 minutes. The principal photons useful for imaging are the dual 511 keV gamma photons, that are produced and emitted simultaneously in opposite direction when the positron interacts with an electron (Table 2).

Table 2. Pricipal Radiation Emission Data for Fluorine F18

Radiation/Emission	% Per Disintegration	Mean Energy
Positron (b+)	96.73	249.8 keV
Gamma (±)*	193.46	511.0 keV

*Produced by positron annihilation

From: Kocher, D.C. Radioactive Decay Tables DOE/TIC-I 1026, 89 (1981)

The specific gamma ray constant (point source air kerma coefficient) for fluorine F 18 is 5.7 R/hr/mCi (1.35 x 10-6 Gy/hr/kBq) at 1 cm. The half-value layer (HVL) for the 511 keV photons is 4 mm lead (Pb). The range of attenuation coefficients for this radionuclide as a function of lead shield thickness is shown in Table 3. For example, the interposition of an 8 mm thickness of Pb, with a coefficient of attenuation of 0.25, will decrease the external radiation by 75%.

Table 3. Radiation Attenuation of 511 keV Photons by lead (Pb) shielding

Shield thickness (Pb) mm	Coefficient of attenuation
0	0.00
4	0.50
8	0.25
13	0.10
26	0.01
39	0.001
52	0.0001

For use in correcting for physical decay of this radionuclide, the fractions remaining at selected intervals after calibration are shown in Table 4.

Table 4. Physical Decay Chart for Fluorine F18

Minutes	Fraction Remaining
0*	1.000
15	0.909
30	0.826
60	0.683
110	0.500
220	0.250

*calibration time

12 CLINICAL PHARMACOLOGY

12.1 Mechanism of Action

Fludeoxyglucose F 18 is a glucose analog that concentrates in cells that rely upon glucose as an energy source, or in cells whose dependence on glucose increases under pathophysiological conditions. Fludeoxyglucose F 18 is transported through the cell membrane by facilitative glucose transporter proteins and is phosphorylated within the cell to [^{18}F] FDG-6-phosphate by the enzyme hexokinase. Once phosphorylated it cannot exit until it is dephosphorylated by glucose-6-phosphatase. Therefore, within a given tissue or pathophysiological process, the retention and clearance of Fludeoxyglucose F 18 reflect a balance involving glucose transporter, hexokinase and glucose-6-phosphatase activities. When allowance is made for the kinetic differences between glucose and Fludeoxyglucose F 18 transport and phosphorylation (expressed as the ‚lumped constant" ratio), Fludeoxyglucose F 18 is used to assess glucose metabolism.

In comparison to background activity of the specific organ or tissue type, regions of decreased or absent uptake of Fludeoxyglucose F 18 reflect the decrease or absence of glucose metabolism. Regions of increased uptake of Fludeoxyglucose F 18 reflect greater than normal rates of glucose metabolism.

12.2 Pharmacodynamics

Fludeoxyglucose F 18 Injection is rapidly distributed to all organs of the body after intravenous administration. After background clearance of Fludeoxyglucose F 18 Injection, optimal PET imaging is generally achieved between 30 to 40 minutes after administration.

In cancer, the cells are generally characterized by enhanced glucose metabolism partially due to (1) an increase in activity of glucose transporters, (2) an increased rate of phosphorylation activity, (3) a reduction of phosphatase activity or, (4) a dynamic alteration in the balance among all these processes. However, glucose metabolism of cancer as reflected by Fludeoxyglucose F 18 accumulation shows considerable variability. Depending on tumor type, stage, and location, Fludeoxyglucose F 18 accumulation may be increased, normal, or decreased. Also, inflammatory cells can have the same variability of uptake of Fludeoxyglucose F 18.

In the heart, under normal aerobic conditions, the myocardium meets the bulk of its energy requirements by oxidizing free fatty acids. Most of the exogenous glucose taken up by the myocyte is converted into glycogen. However, under ischemic conditions, the oxidation of free fatty acids decreases, exogenous glucose becomes the preferred myocardial sub strate, glycolysis is stimulated, and glucose taken up by the myocyte is metabolized immediately instead of being converted into glycogen. Under these condi-

tions, phosphorylated Fludeoxyglucose F 18 accumulates in the myocyte and can be detected with PET imaging.

In the brain, cells normally rely on aerobic metabolism. In epilepsy, the glucose metabolism varies. Generally, during a seizure, glucose metabolism increases. Interictally, the seizure focus tends to be hypometabolic.

12.3 Pharmacokinetics

Distribution: In four healthy male volunteers, receiving an intravenous administration of 30 seconds in duration, the arterial blood level profile for Fludeoxyglucose F 18 decayed triexponentially. The effective half-life ranges of the three phases were 0.2 to 0.3 minutes, 10 to 13 minutes with a mean and standard deviation (STD) of 11.6 (±) 1.1 min, and 80 to 95 minutes with a mean and STD of 88 (±) 4 min.

Plasma protein binding of Fludeoxyglucose F 18 has not been studied.

Metabolism: Fludeoxyglucose F 18 is transported into cells and phosphorylated to [^{18}F]-FDG-6- phosphate at a rate proportional to the rate of glucose utilization within that tissue. [F18]-FDG-6-phosphate presumably is metabolized to 2-deoxy-2-[F18]fluoro-6-phospho-D-mannose([F 18]FDM-6-phosphate).

Fludeoxyglucose F 18 Injection may contain several impurities (e.g., 2-deoxy-2-chloro-D-glucose (ClDG)). Biodistribution and metabolism of ClDG are presumed to be similar to Fludeoxyglucose F 18 and would be expected to result in intracellular formation of 2-deoxy-2-chloro-6-phospho-D-glucose (ClDG-6-phosphate) and 2-deoxy-2-chloro-6-phospho-D-mannose (ClDM-6-phosphate). The phosphorylated deoxyglucose compounds are dephosphorylated and the resulting compounds (FDG, FDM, ClDG, and ClDM) presumably leave cells by passive diffusion. Fludeoxyglucose F 18 and related compounds are cleared from non-cardiac tissues within 3 to 24 hours after administration. Clearance from the cardiac tissue may require more than 96 hours. Fludeoxyglucose F 18 that is not involved in glucose metabolism in any tissue is then excreted in the urine.

Elimination: Fludeoxyglucose F 18 is cleared from most tissues within 24 hours and can be eliminated from the body unchanged in the urine. Three elimination phases have been identified in the reviewed literature. Within 33 minutes, a mean of 3.9% of the administrated radioactive dose was measured in the urine. The amount of radiation exposure of the urinary bladder at two hours post-administration suggests that 20.6% (mean) of the radioactive dose was present in the bladder.

Special Populations:

The pharmacokinetics of Fludeoxyglucose F 18 Injection have not been studied in renally-impaired, hepatically impaired or pediatric patients. Fludeoxyglucose F 18 is eliminated through the renal system. Avoid excessive radiation exposure to this organ system and adjacent tissues.

The effects of fasting, varying blood sugar levels, conditions of glucose intolerance, and diabetes mellitus on Fludeoxyglucose F 18 distribution in humans have not been ascertained [see Warnings and Precautions (5.2)].

13 NONCLINICAL TOXICOLOGY

13.1 Carcinogenesis, Mutagenesis, Impairment of Fertility

Animal studies have not been performed to evaluate the Fludeoxyglucose F 18 Injection carcinogenic potential, mutagenic potential or effects on fertility.

14 CLINICAL STUDIES

14.1 Oncology

The efficacy of Fludeoxyglucose F 18 Injection in positron emission tomography cancer imaging was demonstrated in 16 independent studies. These studies prospectively evaluated the use of Fludeoxyglucose F 18 in patients with suspected or known malignancies, including non-small cell lung cancer, colo-rectal, pancreatic, breast, thyroid, melanoma, Hodgkin's and non-Hodgkin's lymphoma, and various types of metastatic cancers to lung, liver, bone, and axillary nodes. All these studies had at least 50 patients and used pathology as a standard of truth. The Fludeoxyglucose F 18 Injection doses in the studies ranged from 200 MBq to 740 MBq with a median and mean dose of 370 MBq.

In the studies, the diagnostic performance of Fludeoxyglucose F 18 Injection varied with the type of cancer, size of cancer, and other clinical conditions. False negative and false positive scans were observed. Negative Fludeoxyglucose F 18 Injection PET scans do not exclude the diagnosis of cancer. Positive Fludeoxyglucose F 18 Injection PET scans can not replace pathology to establish a diagnosis of cancer. Non-malignant conditions such as fungal infections, inflammatory processes and benign tumors have patterns of increased glucose metabolism that may give rise to false-positive scans. The efficacy of Fludeoxyglucose F 18 Injection PET imaging in cancer screening was not studied.

14.2 Cardiology

The efficacy of Fludeoxyglucose F 18 Injection for cardiac use was demonstrated in ten independent, prospective studies of patients with coronary artery disease and chronic left ventricular systolic dysfunction who were scheduled to undergo coronary revascularization. Before revascularization, patients underwent PET imaging with Fludeoxyglucose F 18 Injection (74 to 370 MBq, 2 to 10 mCi) and perfusion imaging with other diagnostic radiopharmaceuticals. Doses of Fludeoxyglucose F 18 Injection ranged from 74 to 370 MBq (2 to 10 mCi). Segmental, left ventricular, wall-motion assessments of asynergic areas made before revascularization were compared in a blinded manner to assessments made after successful revascularization to identify myocardial segments with functional recovery.

Left ventricular myocardial segments were predicted to have reversible loss of systolic function if they showed Fludeoxyglucose F 18 accumulation and reduced perfusion (i.e., flow-metabolism mismatch). Conversely, myocardial segments were predicted to have irreversible loss of systolic function if they showed reductions in both Fludeoxyglucose F 18 accumulation and perfusion (i.e., matched defects).

Findings of flow-metabolism mismatch in a myocardial segment may suggest that successful revascularization will restore myocardial function in that segment. However, false-positive tests occur regularly, and the decision to have a patient undergo revascularization should not be based on PET findings alone. Similarly, findings of a matched defect in a myocardial segment may suggest that myocardial function will not recover in that segment, even if it is successfully revascularized. However, false-negative tests occur regularly, and the decision to recommend against coronary revascularization, or to recommend a cardiac transplant, should not be based on PET findings alone. The reversibility of segmental dysfunction as predicted with Fludeoxyglucose F 18 PET imaging depends on successful coronary revascularization. Therefore, in patients with a low likelihood of successful revascularization, the diagnostic usefulness of PET imaging with Fludeoxyglucose F 18 Injection is more limited.

14.3 Neurology

In a prospective, open label trial, Fludeoxyglucose F 18 Injection was evaluated in 86 patients with epilepsy. Each patient received a dose of Fludeoxyglucose F 18 Injection in the range of 185 to 370 MBq (5 to 10 mCi). The mean age was 16.4 years (range: 4 months to 58 years; of these, 42 patients were less than 12 years and 16 patients were less than 2 years old). Patients had a known diagnosis of complex partial epilepsy and were under evaluation for surgical treatment of their seizure disorder. Seizure foci had been previously identified on ictal EEGs and sphenoidal EEGs. Fludeoxyglucose F 18 Injection PET imaging confirmed previous diagnostic findings in 16% (14/87) of the patients; in 34% (30/87) of the patients, Fludeoxyglucose F 18 Injection PET images provided new findings. In 32% (27/87), imaging with Fludeoxyglucose F 18 Injection was inconclusive. The impact of these imaging findings on clinical outcomes is not known.

Several other studies comparing imaging with Fludeoxyglucose F 18 Injection results to subsphenoidal EEG, MRI and/or surgical findings supported the concept that the degree of hypometabolism corresponds to areas of confirmed epileptogenic foci. The safety and effectiveness of Fludeoxyglucose F 18 Injection to distinguish idiopathic epileptogenic foci from tumors or other brain lesions that may cause seizures have not been established.

15 REFERENCES

1. Gallagher B.M., Ansari A., Atkins H., Casella V., Christman D.R., Fowler J.S., Ido T., MacGregor R.R., Som P., Wan C.N., Wolf A.P., Kuhl D.E., and Reivich M. "Radiopharmaceuticals XXVII. 18F-labeled 2-deoxy-2-fluoro-d-glucose as a radiopharmaceutical for measuring regional myocardial glucose metabolism in vivo: tissue distribution and imaging studies in animals," J Nucl Med, 1977; 18, 990-6.
2. Jones S.C., Alavi, A., Christman D., Montanez, I., Wolf, A.P., and Reivich M. "The radiation dosimetry of 2 [F-18] fluoro-2-deoxy-D-glucose in man," J Nucl Med, 1982; 23, 613-617.
3. Kocher, D.C. "Radioactive Decay Tables: A handbook of decay data for application to radiation dosimetry and radiological assessments," 1981, DOE/TIC-I 1026, 89.
4. ICRP Publication 53, Volume 18, No. I-4,1987, pages 75-76.

16 HOW SUPPLIED/STORAGE AND DRUG HANDLING

Fludeoxyglucose F 18 Injection is supplied in a multi-dose, capped 30 mL and 50 mL glass vial containing between 0.740 to 7.40 GBq/mL (20 to 200 mCi/mL), of no carrier added 2-deoxy-2-[F 18] fluoro-D-glucose, at end of synthesis, in approximately 15 to 50 mL. The contents of each vial are sterile, pyrogen-free and preservative-free.

NDC 40028-511-30; 40028-511-50

Receipt, transfer, handling, possession, or use of this product is subject to the radioactive material regulations and licensing requirements of the U.S. Nuclear Regulatory Commission, Agreement States or Licensing States as appropriate.

Store the Fludeoxyglucose F 18 Injection vial upright in a lead shielded container at 25°C (77°F); excursions permitted to 15-30°C (59-86°F).

Store and dispose of Fludeoxyglucose F 18 Injection in accordance with the regulations and a general license, or its equivalent, of an Agreement State or a Licensing State.

The expiration date and time are provided on the container label. Use Fludeoxyglucose F 18 Injection within 12 hours from the EOS time.

17 PATIENT COUNSELING INFORMATION

Instruct patients in procedures that increase renal clearance of radioactivity. Encourage patients to:

- drink water or other fluids (as tolerated) in the 4 hours before their PET study.
- void as soon as the imaging study is completed and as often as possible thereafter for at least one hour.

Manufactured by: PETNET Solutions Inc.
810 Innovation Drive
Knoxville, TN 37932

Distributed by: PETNET Solutions Inc.
810 Innovation Drive
Knoxville, TN 37932

PETNET Solutions

PN0002262 Rev. A
March 1, 2011

On account of certain regional limitations of sales rights and service availability, we cannot guarantee that all products included in this brochure are available through the Siemens sales organization worldwide. Availability and packaging may vary by country and is subject to change without prior notice. Some/All of the features and products described herein may not be available in the United States.

The information in this document contains general technical descriptions of specifications and options as well as standard and optional features which do not always have to be present in individual cases.

Siemens reserves the right to modify the design, packaging, specifications and options described herein without prior notice.

Please contact your local Siemens sales representative for the most current information.

Note: Any technical data contained in this document may vary within defined tolerances. Original images always lose a certain amount of detail when reproduced.

Local Contact Information

Asia/Pacific:
Siemens Medical Solutions
Asia Pacific Headquarters
The Siemens Center
60 MacPherson Road
Singapore 348615
Phone: +65 9622-2026
www.siemens.com/healthcare

Canada:
Siemens Canada Limited
Medical Solutions
2185 Derry Road West
Mississauga ON L5N 7A6
Canada
Phone: +1 905 819-5800
www.siemens.com/healthcare

Europe/Africa/Middle East:
Siemens AG
Medical Solutions
Henkestraße 127
D-91052 Erlangen
Germany
Phone: +49 9131 84-0
www.siemens.com/healthcare

Latin America:
Siemens S.A.
Medical Solutions
Avenida de Pte. Julio A. Roca No 516, Piso 7
C1067ABN Buenos Aires Argentina
Phone: +54 11 4340-8400
www.siemens.com/healthcare

USA:
Siemens Medical Solutions USA, Inc.
51 Valley Stream Parkway
Malvern, PA 19355-1406
USA
Phone: +1-888-826-9702
www.siemens.com/healthcare

Global Siemens Headquarters

Siemens AG
Wittelsbacherplatz 2
80333 Muenchen
Germany

Global Siemens Healthcare Headquarters

Siemens AG
Healthcare Sector
Henkestraße 127
91052 Erlangen
Germany
Phone: +49 9131 84-0
www.siemens.com/healthcare

www.siemens.com/imaginglife